Received: 21 December 2020 | Accepted: 27 January 2021

DOI: 10.1111/bre.12555

RESEARCH ARTICLE

Basin Research IAS EAGE WILEY

Mixed axial and transverse deep-water systems: The Cretaceous post-rift Lysing Formation, offshore Norway

L. A. S. Hansen[1] | **D. M. Hodgson**[1] | **A. Pontén**[2] | **C. Thrana**[2] | **A. Obradors Latre**[3]

[1]School of Earth and Environment, University of Leeds, Leeds, UK

[2]Equinor, Research Centre Rotvoll, Equinor ASA, Trondheim, Norway

[3]Equinor, Research Centre Bergen, Equinor ASA, Sandsli, Norway

Correspondence
Larissa Hansen, School of Earth and Environment, University of Leeds, UK.
Email: l.a.hansen@leeds.ac.uk

Funding information
Equinor ASA

Abstract

Deep-water stratigraphic successions from syn- to post-rift stages are an archive of evolving physiographic configurations, and can record axial and transverse sedimentary sources. The healing of topography decreases the influence of syn-rift structures on sedimentation patterns and transport processes over time, which leads to a long-term transition from dominantly axial to transverse dispersal patterns. The Halten and Dønna terraces, offshore mid-Norway, comprise a series of rift-related sub-basins established during the Jurassic, which were infilled with sediments during the Cretaceous. The Cretaceous Lysing Formation developed as slope- and basin-floor fans within a series of weakly confined post-rift sub-basins with some shallow marine deposits interpreted on the basin margins. A deep-water setting is supported by seismic interpretation, and bed type and architectural element analysis in all cored and uncored wells in the area. We document that an axial submarine fan system was active throughout the post-rift stage due to subtle inherited topography from syn-rift structures, which interacted with locally sourced transverse sediment sources. This led to a complicated stratigraphic architecture, with lobe fringe deposits of the axial fan system juxtaposed with channel-fills and channel-lobe transition zone deposits of transverse systems. The refined palaeogeographic reconstruction of the Lysing Formation illustrates how subtle topography can impact sediment routing patterns many millions of years after the end of rifting and can be used for palaeoenvironmental interpretations in other post-rift settings.

KEYWORDS

channel-lobe-transition-zone, lysing formation, Norway, palaeogeographic reconstruction, post-rift, submarine lobes

Highlights

- Interaction of axial and transverse deep-water systems in post-rift settings.
- Subtle topography impacts sediment routing patterns in post-rift settings.
- Channel-lobe transition zone deposits observed in core indicating scour- or distributary channel-fills.

1 | INTRODUCTION

The evolving physiographic configurations and sediment routing patterns of deep-water systems in rift basins are characterized by the decreasing influence of syn-rift structures through time (Hadlari et al., 2016; McArthur et al., 2016; Muravchik et al., 2020). Syn- to post-rift tectono-stratigraphic models emphasize limited thickness and facies variations across structures in a late post-rift setting (Hadlari et al., 2016; Leinfelder, Wilson, & Chris 1998; Prosser, 1993). Several subsurface studies have documented the distribution and morphology of early post-rift sand fairways and sand-rich fans accumulated across inherited rift structures (Fjellanger et al., 2005; Fugelli & Olsen, 2007; Jackson et al., 2008; Martinsen et al., 2005). However, few studies have documented the detailed architecture and facies distribution in post-rift systems (Dodd, McCarthy, & Richards, 2019; Haughton, Barker, & McCaffrey,, 2003; Southern et al., 2017). The record of interplay of controls such as inherited rift physiography, accommodation patterns, and changes in sediment source during the syn- to post-rift transition are poorly understood. Traditionally, Jurassic pre-rift hydrocarbon reservoirs have been the focus in the Halten and Dønna terraces, offshore mid-Norway (Figure 1). However, now there is active exploration in the shallower post-rift Cretaceous successions, such as the Lysing Formation, which is interpreted to comprise slope and basin-floor fans within a series of weakly confined post-rift sub-basins (Fugelli & Olsen, 2007; Martinsen et al., 2005). The combination of decreasing but differential subsidence, controlled by underlying Jurassic structures, and overall eustatic sea-level rise formed low relief accommodation on a gentle regional deep-water slope (Martinsen et al., 2005). This study utilizes data from all available cored and a selection of uncored wells on the Halten and Dønna terraces (Figure 1B) to interpret the architectural elements in each well with the aim to develop a regional-scale deep-water post rift model across a 25,000 km^2 basin area. An enigmatic facies association described by multiple studies before (Fugelli & Olsen, 2007; Lien et al., 2006; Martinsen et al., 2005; Shanmugam et al., 1994) is reinterpreted based on new seismic and well data, and highlights the interaction between a large axial submarine fan system that was coeval with locally sourced transverse sediment sources. Furthermore, we emphasize that inherited and compaction-enhanced rift topography can influence sediment routing patterns and basin-fill architecture well past the cessation of the rifting period during late post-rift stages, which can also be applied to other post-rift basins. An improved understanding of the depositional environment will enable better reservoir sand prediction for upcoming exploration and development targets.

2 | GEOLOGICAL AND STRATIGRAPHIC SETTING

The Halten and Dønna terraces are located on the Norwegian continental shelf at 64°–66° N, between the Trøndelag Platform in the east and the Vøring Basin in the west (Figure 1). The structural history involves multiple extensional phases during the Palaeozoic, Mesozoic and earliest Cenozoic that culminated in the separation of Greenland and Norway during the Early Cenozoic (Brekke et al., 1999; Mosar et al., 2002; Torsvik & Cocks, 2005). Several inversion episodes occurred during the Cenozoic (Brekke et al., 2001; Doré & Lundin, 1996; Skogseid et al., 2000; Swiecicki et al., 1998).

The Halten and Dønna terraces separated from the Trøndelag Platform in the Late Cretaceous (Brekke et al., 1999) (Figure 1). Reactivation of older faults along basin-bounding platforms resulted in the separation of the Dønna Terrace from the Nordland Ridge, and the southern part of the Nordland Ridge was subjected to uplift and faulting. Several unconformities suggest that the Nordland Ridge existed as an emergent high throughout the Cretaceous (Hastings, 1987). The Dønna Terrace is roughly diamond-shaped and faults subdivide the terrace into a series of half grabens of irregular shape and variable width and length, gradually downstepping towards the Rås and Vøring Basin in the west (Figure 1). The Halten and Dønna terraces are separated by the Heidrun-Smørbukk fault zone, a northeast-southwest–trending complex transfer zone consisting of local narrow horst blocks, grabens, and half grabens (Gawthorpe & Hurst, 1993; Gibbs, 1984; Morley et al., 1990) (Figure 1B). The Halten terrace is separated from the Trøndelag platform by a 10-km-wide zone of normal faults (Figure 1B) (Elliott et al., 2012).

The inherited Late Jurassic syn-rift basin topography was progressively filled during the Early Cretaceous post-rift phase (lower Lange Formation), which was dominated by deposition of muds (Figure 2) (Færseth & Lien, 2002). During the Cenomanian to lower Turonian sediment supply increased, but the sand-prone Lange Formation was still influenced by inherited syn-rift topography (Brekke et al., 2001; Færseth & Lien, 2002). In the middle to upper Turonian, after abandonment of the sandstone-prone Lange Formation, the influence of syn-rift topography decreased during the deposition of bioturbated and laminated muds (Brekke et al., 2001; Færseth & Lien, 2002). In the upper Turonian to lower Coniacian, the sandstone-prone Lysing Formation was deposited, during continued differential subsidence above Jurassic syn-rift structures that maintained low relief accommodation and gentle intrabasinal slopes (Færseth & Lien, 2002) (Figure 2). The stratigraphic framework of the Cretaceous sediments on the Halten and Dønna terraces is based on the biostratigraphic calibration of several maximum flooding surfaces and unconformities. A prominent high gamma ray spike near the base of the Lysing Formation defines a consistent stratigraphic framework for the Lysing Formation sandstones. The top of the Lysing Formation is defined at the top of the sandstone interval, which also marks the top of the Cromer Knoll Group.

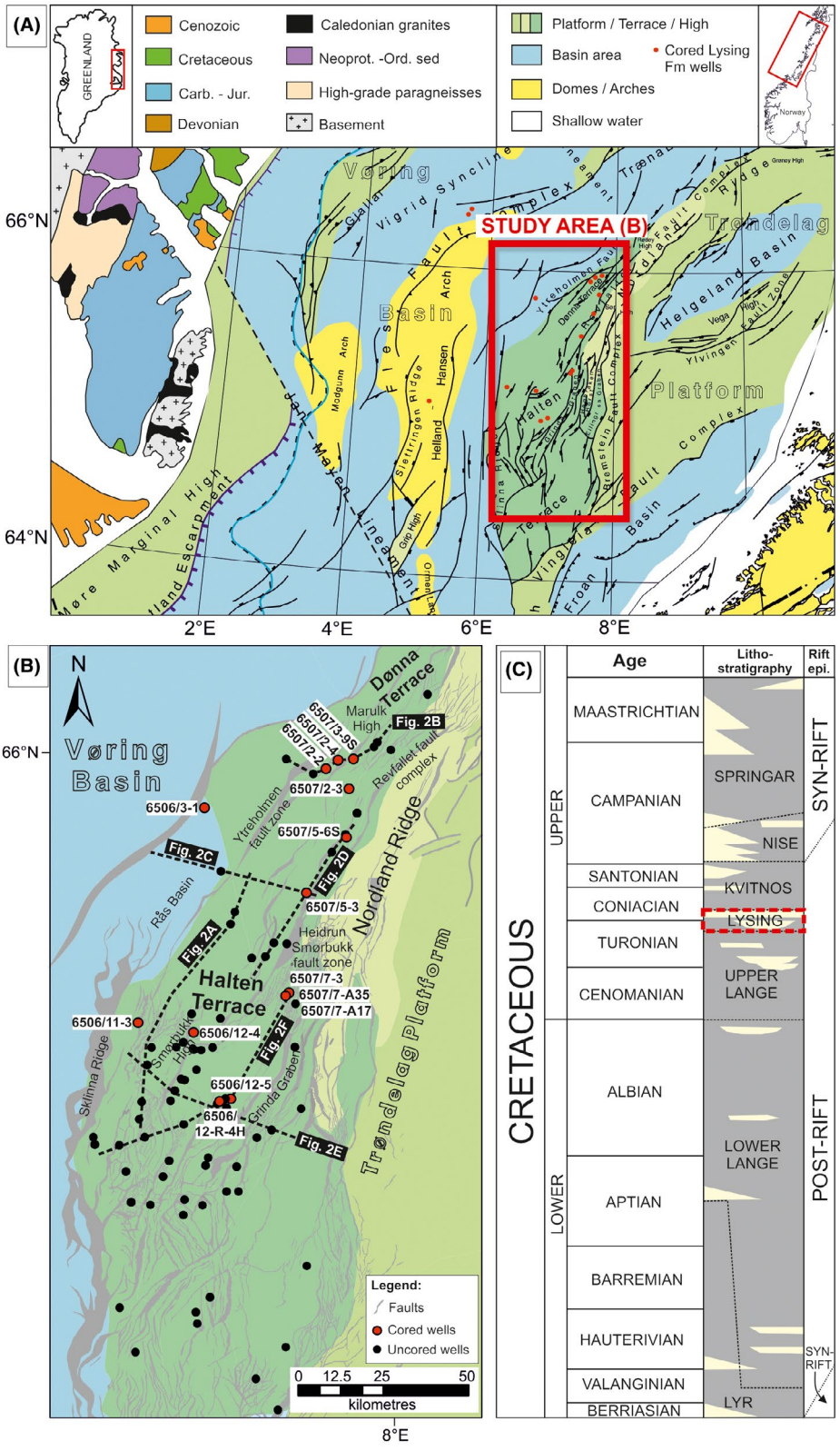

FIGURE 1 (A) Structural elements of the platforms and basins within the Norwegian continental sea and a simplified geological map of the East Greenland margin (modified Blystad et al., 1995; Fonneland et al., 2004). The pre-drift reconstruction shows the position of East Greenland along the western margin of the Vøring Basin during the Cretaceous period (after Fonneland et al., 2004). (B) Study area highlighted in a) with wells included in this study indicated by the red and black dots. Seismic cross sections shown in Figure 2 are also highlighted by black dashed lines. (C) Stratigraphic column of the Cretaceous in the Norwegian Sea with the Lysing Formation highlighted in the red square

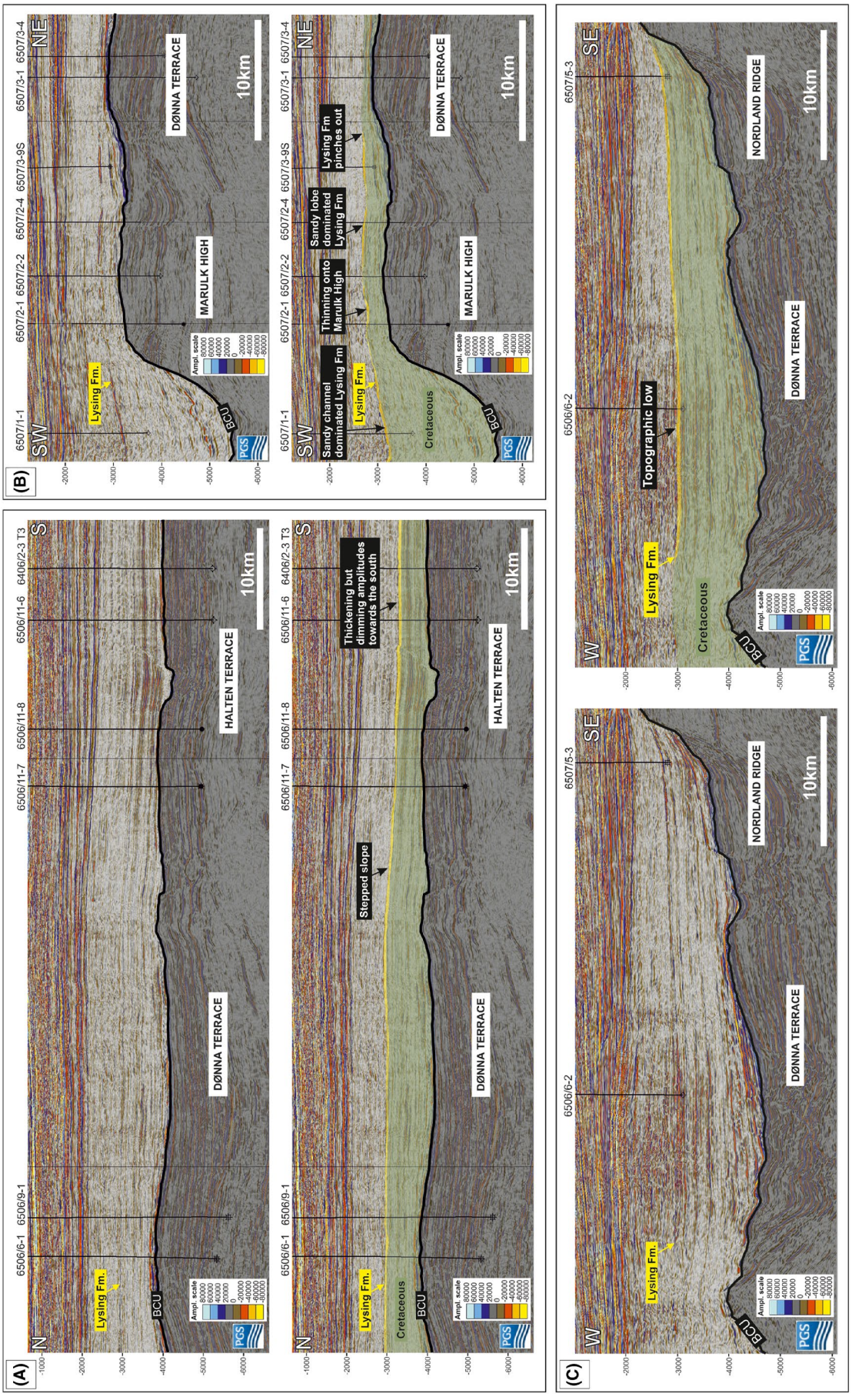

FIGURE 2 Regional seismic reflection lines indicating the infilling of the Jurassic syn-rift topography (marked in grey with the top indicated by the Base Cretaceous Unconformity (BCU)) by Cretaceous sediments (marked in green). The Lysing Formation is indicated in yellow. Locations of the seismic cross sections are shown in Figures 1B and 3A

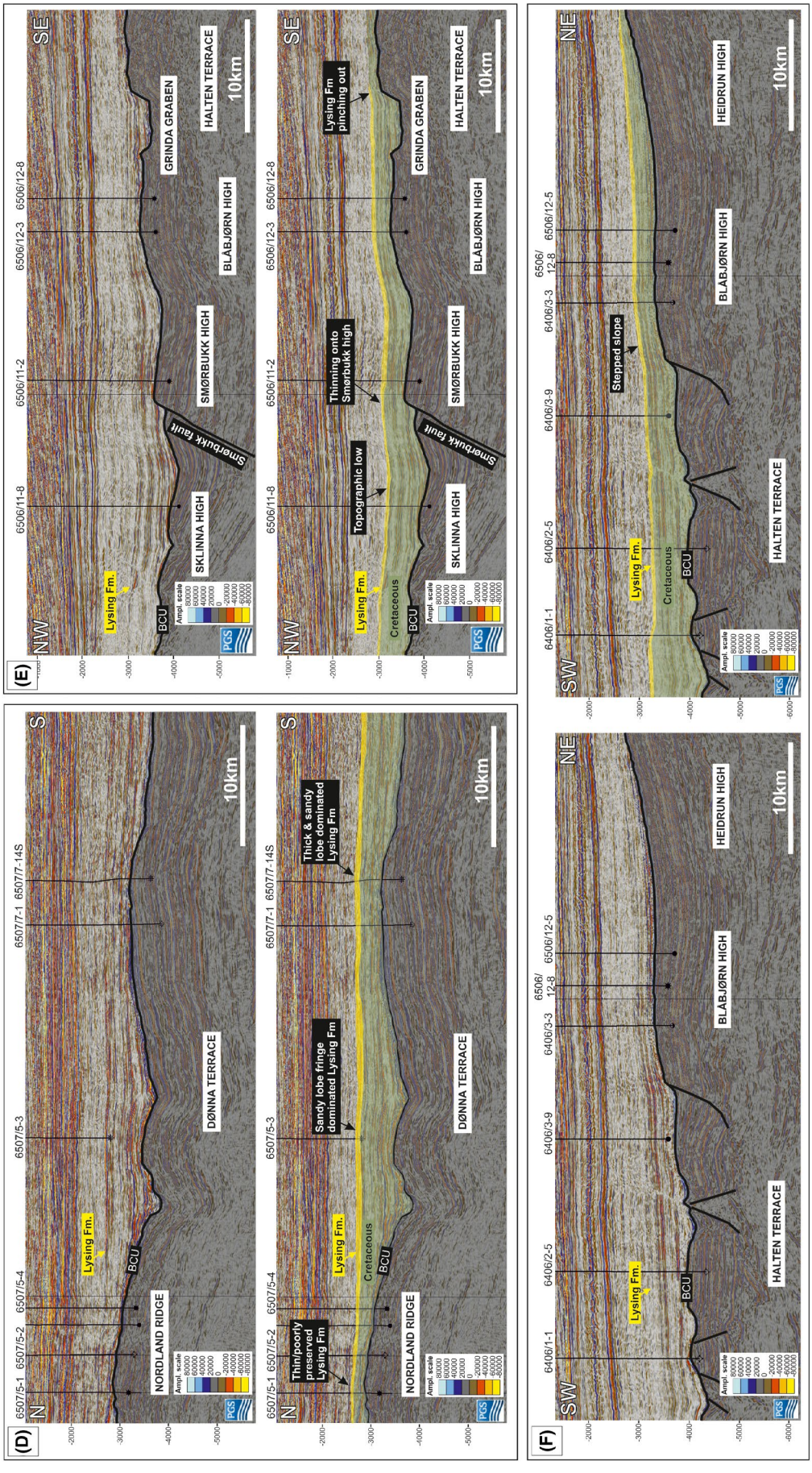

FIGURE 2 Continued

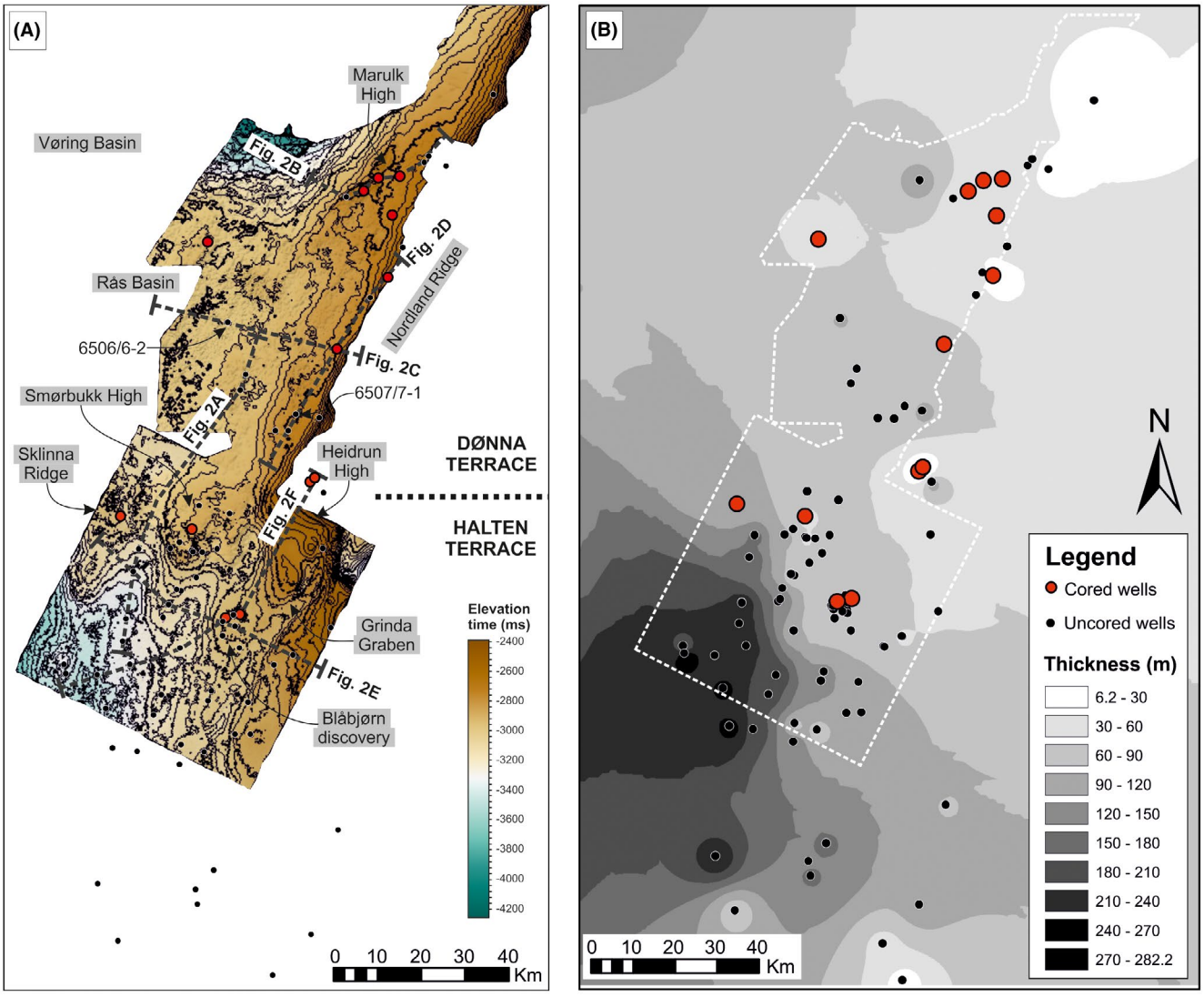

FIGURE 3 (A) Regional depth map of the Lysing Formation indicating the main structural elements and the location of seismic lines in Figure 2. (B) Isochore map of the Lysing Formation based on well thicknesses. For orientation purposes, the outline of the depth map is shown by the white dashed line

3 | METHODOLOGY AND DATA SET

This study is based on 14 cored (a total of 344 m of core) and 92 uncored wells from the Lysing Formation across a 25,000 km^2 area on the Halten and Dønna terraces (Figure 1). A combination of core, well logs (gamma ray, neutron, density), biostratigraphy and seismic stratigraphy were used to define the top and base of the Lysing Formation. Core logs recorded data on lithology, sedimentary structures, bed thickness, percentage of glauconite, bioturbation intensity and cementation. Selected thin-sections were used to help with the glauconite identification and quantification. Logs were collected at 1:5 scale. The description and interpretation of the cores involved the classification of sedimentary facies, bed types and architectural elements. An architectural element is a sedimentary body defined by its geometry (including orientation), scale, bounding surfaces, and bed types (Pickering et al., 1995). Individual bed types can be a component of multiple architectural elements. The abundance and stacking patterns of bed types, combined with the scale and geometry of sedimentary bodies on seismic data, support architectural element interpretations. The architectural elements were calibrated between core and well logs, prior to interpretation of the architectural elements in the uncored wells. Well log quality varied and many wells are drilled on structural highs targeting the sandier intervals of the formation, which made the use of regional 3D seismic reflection data crucial to generate a Lysing Formation depth map and support the interpretation of the depositional environment. A supermerge of two broadband 3D seismic cubes was pre-stack depth migrated (PSDM VTI Kirchhoff) and post-stack noise removal applied. The data were reprocessed to reduce noise and remove multiples which improved the signal to noise ratio at the Cretaceous stratigraphic level. The vertical resolution for the stratigraphic interval of interest is estimated to be 20 m. Seismic

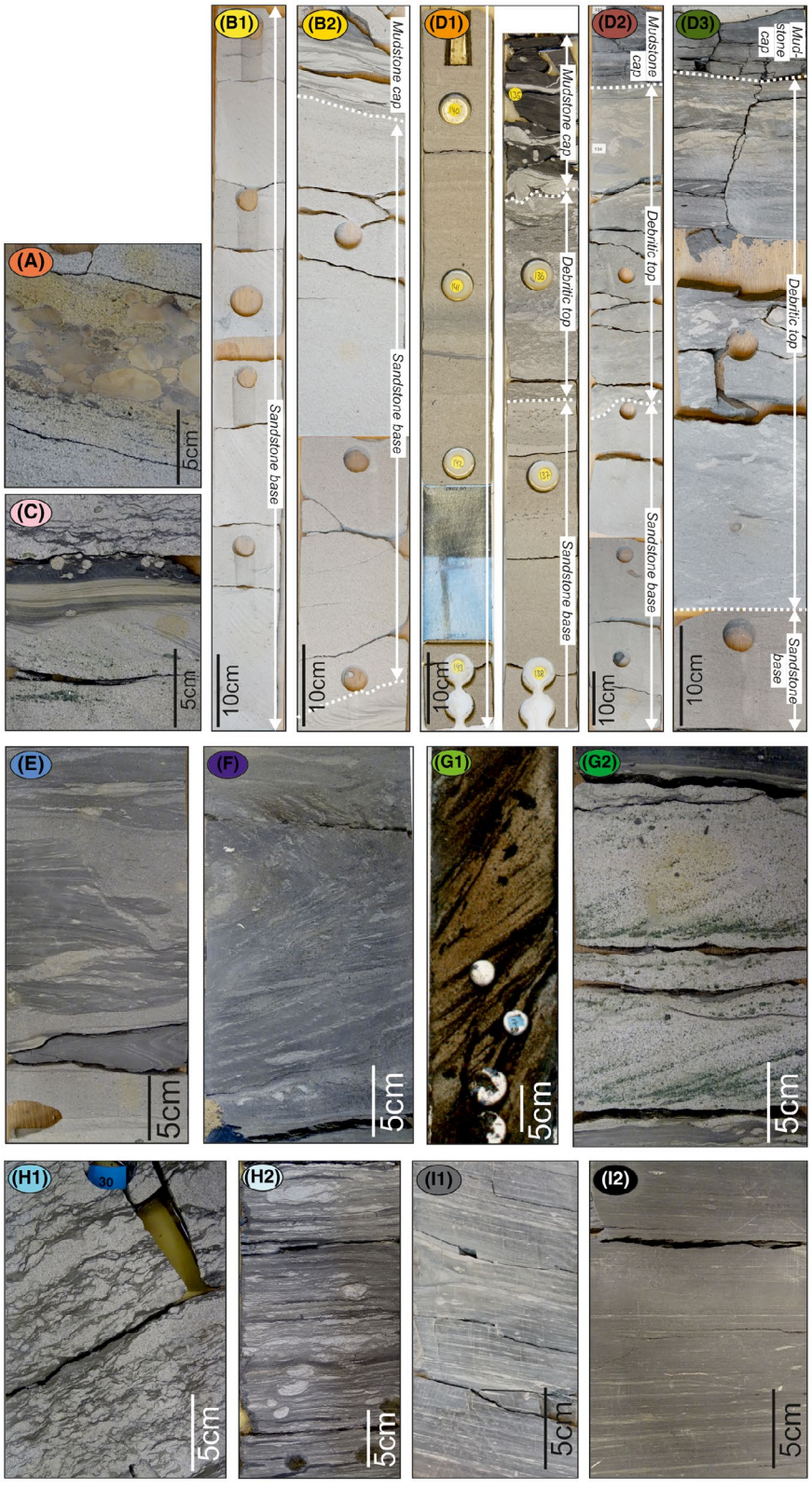

FIGURE 4 Lysing Formation bed types. Labelling corresponds to bed types described in Table 1. A—Clast supported conglomerate, B1—Amalgamated structureless thick-bedded sandstone, B2—Thick-bedded structured sandstone, C—Thin-bedded structured sandstone, D1—Sand-rich bipartite bed, D2—Argillaceous sand-prone bipartite bed, D3—Mud-prone bipartite bed, E—Poorly sorted sandy mudstones, F—Folded strata, G1—Cross-stratified sandstones with mud drapes, G2—Cross-stratified glauconitic sandstones, H1—Bioturbated sandy heterolithics, H2—Bioturbated silty heterolithics, I1—Bioturbated mudstone, I2—Laminated mudstone

stratigraphic surfaces were interpreted by identifying regionally extensive impedance boundaries associated with truncation, concordance, onlap and offlap within the Cromer Knoll Group. In order to constrain lithology and time relationships, the seismic stratigraphic surfaces where calibrated with biostratigraphy, well log signatures and observations from core (when available). This enabled the identification of condensed sections and unconformities subdividing the stratigraphy into a

TABLE 1 Lysing Formation bed type scheme including process and architectural element interpretation

Bed type	% of cored Lysing Formation	Thickness range	Description	Process interpretation	Architectural element
Clast-supported conglomeratic (A)	0.4	<15 cm	Extra- and intrabasinal clast-rich sandstone/matrix-supported conglomerate. Matrix supported and cemented mudclast conglomerate. Generally poorly sorted	Bedload deposits below high-density turbidity currents. Typically represent sediment bypass lags (Stevenson et al., 2015)	Distributary channel-fill or submarine channel axis
Amalgamated structureless thick-bedded sandstone (B1)	11.2	>50 cm	More than 50% homogeneous sandstone, locally banded, plane parallel and cross-laminated sandstone. Difference in bed types is due to thickness variations	Deposition beneath a high-density turbidity current with high suspension fallout rates and some tractional reworking of bed tops. Thickness of bed varies with size of flow with amalgamated beds produced by flows eroding into previous bed	Submarine channel axis or margin, or lobe axis
Thick-bedded structured sandstone (B2)	0.4	10–50 cm			Submarine channel axis or margin, or lobe axis or lobe off-axis
Thin-bedded structured sandstone (C)	0.8	<10 cm	Fine grained sandstone to siltstone, more than 50% fine grained ripple laminated sandstone	Deposition by a low-density turbidity current with sedimentary structures produced by dilute flows that tractionally rework the bed top. Bed thickness determined by flow size	Channel, margin, overbank, abandonment, lobe off-axis, distal frontal lobe fringe, frontal lobe fringe, lateral lobe fringe
Sand-rich bipartite bed (D1)	20	40–350 cm	More than 85% dewatered sandstone, with some banded or plane parallel sandstone. Dewatered argillaceous, ripple laminated sandstone below the mudstone top of the bed	Initial deposition from relatively non-cohesive flow. Significant deposition from near-bed flow that fluctuated between turbulent and relatively more cohesive states. Final deposition from cohesive quasi-laminar flow forming sandstone-prone hybrid beds	Frontal lobe fringe
Argillaceous sand-prone bipartite bed (D2)	8.4	50–350 cm	50%–85% dewatered sandstone, with some banded or plane parallel sandstone. Thicker dewatered argillaceous, ripple laminated sandstone below the mudstone top of the bed	Increased deposition beneath cohesive, quasi laminar flow during later stages of deposition forming argillaceous sandstone-prone hybrid beds	Frontal lobe fringe, distal frontal lobe fringe
Mud-prone bipartite bed (D3)	2.9	6–250 cm	Less than 50% dewatered sandstone, with some banded or plane parallel sandstone. Thick dewatered argillaceous, ripple laminated sandstone below the mudstone top of the bed	Dominant deposition beneath cohesive, quasi-laminar flow forming mud-prone hybrid beds	Distal frontal lobe fringe
Poorly sorted sandy mudstones (E)	0.9	15–110 cm	Poorly sorted mudstone to lower medium sandstone with large contorted mudstone clasts. Commonly dewatered with abundant organic matter, some shell fragments and injectites. Lots of sheared pipes and dewatered dishes. Chaotic and debritic texture	*En masse* deposition from debris flows	Channel margin, MTD, distal frontal lobe fringe

(Continues)

TABLE 1 (Continued)

Bed type	% of cored Lysing Formation	Thickness range	Description	Process interpretation	Architectural element
Folded strata (F)	0.2	10–60 cm	Deformed interbedded mudstone, siltstone and sandstone strata. Typically folded or chaotically intermixed	Deposited by remobilization processes forming slides and slumps	Channel margin, MTD
Cross-stratified sandstones with mud drapes (G1)	4.5	10–390 cm	Cross-stratified medium to coarse-grained sandstone with some mud draped bioturbated heterolithics (*Phycosiphon, Ophiomorpha*)	Deposition of sand bedforms that migrated in response to relatively strong currents. Mudstone drapes deposited during slackwater periods	Upper delta front
Cross-stratified glauconitic sandstones (G2)	5	2–100 cm	Commonly cross-stratified, and rarely parallel laminated or structureless sandstones. Glauconite and black opaque grains concentrated on foresets. Some pebble-sized mudclasts. Locally, weakly graded. Sharp erosional tops draped by mudstone. Erosional bases are common	Deposited below high-energy currents able to maintain tractional processes at the bed. The glauconite is interpreted to be reworked and not in-situ and suggests a shelfal source area	CLTZ
Bioturbated sandy heterolithics (H1)	4.8	8–70 cm	Heterolithics composed of siltstone with abundant sandstone beds. Ripple lamination common. Intensely bioturbated with low ichnodiversity (most common are *Nereites, Palaeophycus, Taenidium*)	Deposited by low-density turbidity currents with enough energy to form ripples. Nutrient and oxygen levels were high enough to create conditions ideal for a variety of trace-making organisms. Sandstone-prone heterolithics occur in more proximal settings compared to siltstone-prone heterolithics.	CLTZ, lower delta front, prodelta, abandonment,
Bioturbated silty heterolithics (H2)	15.7	3–550 cm	Heterolithics composed of siltstone and some thin sandstone beds with common starved ripple trains. Intensely bioturbated with high ichnodiversity (*Arenicolites, Artichnus, Chondrites, Nereites, Palaeophycus, Planolites, Scolicia, Skolithos, Teichichnus, Thalassinoides, Zoophycus*)		CLTZ, lower delta front, prodelta, abandonment,
Bioturbated mudstone (I1)	5.7	2–90 cm	Mudstone with some very thin and fine sandstone beds with abundant bioturbation	Background hemipelagic deposition with occasional suspension fall-out from distal dilute turbidity currents introducing enough nutrients and oxygen to the environment to allow bioturbation	Background, lateral lobe fringe
Laminated mudstone (I2)	19	1–1,600 cm	Finely laminated mudstone with minor bioturbation, can be intercalated with siltstone. Can occur as thick packages forming regional mudstone packages or as thin beds	Hemipelagic suspension fallout from the water column	Background, abandonment, CLTZ margin

Abbreviations: CLTZ = channel-lobe transition zone; MTD = mass-transport deposits.

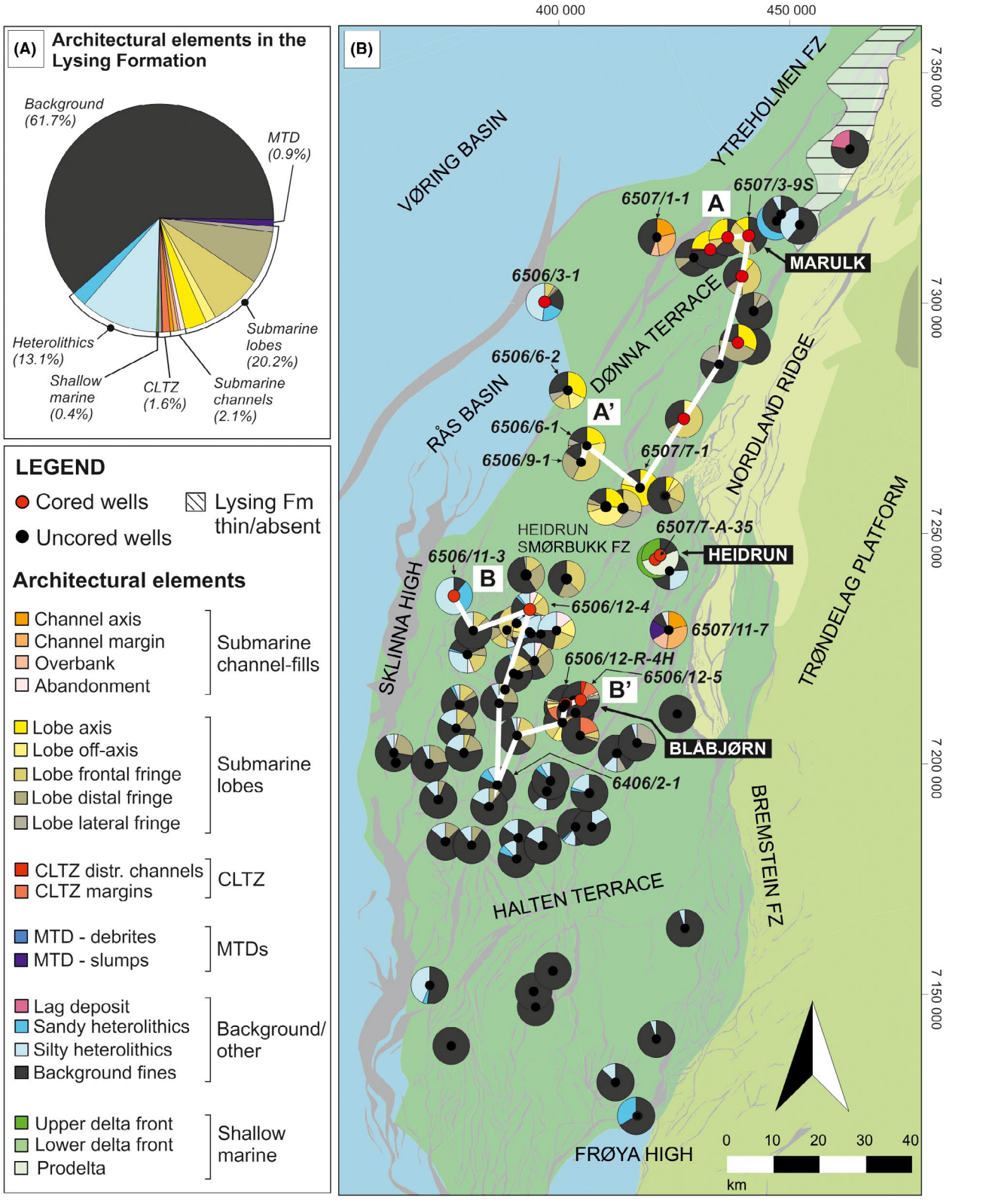

FIGURE 5 (A) Summary of the architectural element distribution in the Lysing Formation including the data from all the cored and uncored wells. (B) Architectural element distribution in the cored and uncored wells with the location of the well cross sections shown in Figure 6 highlighted by the white lines. Wells referred to in the text are labelled

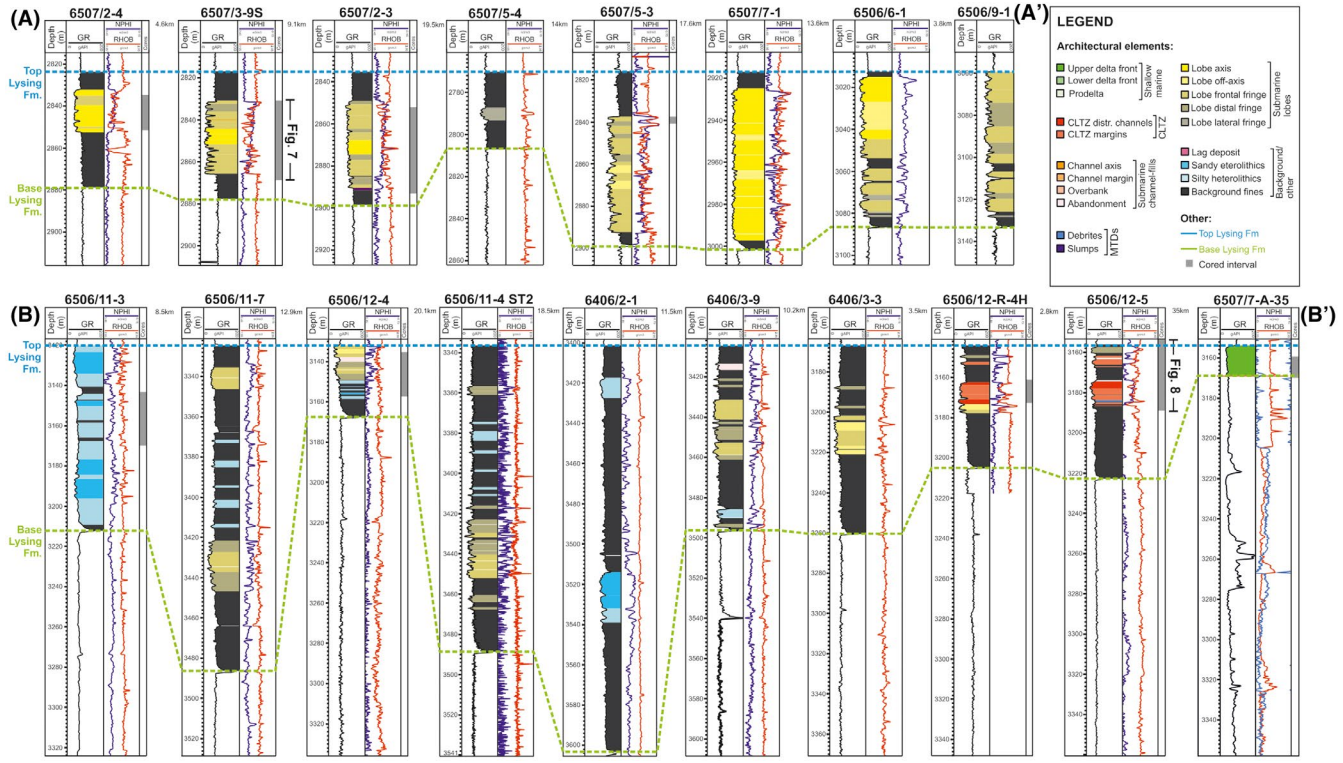

FIGURE 6 Well correlations of key wells (coloured by architectural elements) in the Lysing Formation to illustrate the difference in architectural elements in A) the northern wells and B) the southern wells. The location of correlation panels is shown in Figure 5. The cores shown in Figures 7 and 8 are also indicated

regional chronostratigraphic framework. The spectral decomposition image was created from the full stack seismic data (centre frequencies for RGB blend: 10 Hz for red, 14 Hz for green and 18 Hz for blue) and shows 50 ms above the base Lysing Formation horizon.

4 | TOPOGRAPHIC CONFIGURATION DURING LYSING FORMATION DEPOSITION

The Lysing Formation depth map shows that the Halten and Dønna terraces were bound by the Nordland Ridge to the east and the Rås Basin to the west (Figure 3A). The Halten Terrace was dipping towards the south and south-west with a significant deepening in the southwest of the study area (Figures 2A and 3A). Analysis of the cored and uncored wells shows that the overall thickness of the Lysing Formation varies between 6 m and 282 m, with the thickest part of the formation being in the southwest (Figure 3B) towards the deeper areas.

Using the depth map generated from seismic reflection data, the Dønna Terrace dips towards the west with the Marulk High forming an elevated area in the east next to the Nordland Ridge (Figure 3A). Cretaceous sediments thin onto the Marulk High, and subtle topography on the Marulk High results in thickness variations in the Lysing Formation (Figure 2B). Thickness changes of the Lysing Formation are observed in several locations on the Halten and Dønna terraces. Figure 2C shows a subtle thickening of the Lysing Formation into a topographic low at well 6506/6-2, whereas Figure 2D shows thinning of the Lysing Formation towards the south onto a subtle topographic high at well 6507/7-1 (Figure 3A). The Lysing Formation thickens around well 6507/7-1 even though it is positioned on a high, which is attributed to an additional sediment input point in this area. The Lysing Formation thickens into the topographic low between the Sklinna and Smørbukk highs, which forms a conduit between the Halten and Dønna terraces (Figures 2E and 3A). The isochore map indicates a significant increase in thickness along this topographic low and further to the south-west suggesting that this low may have acted as a conduit for sediment transported to the south-west (Figures 2E and 3B). Slight topographic lows along the stepped slope seen from the Heidrun High towards the Blåbjørn discovery and further south-west also result in an increase in thickness in the Lysing Formation in those areas (Figure 2F).

These thickness changes indicate that a subtle topographic template existed at the time of deposition of the Lysing Formation, which influenced sediment routing and storage patterns. The topographic template was largely inherited from the syn-rift structures that formed during a major rifting event in

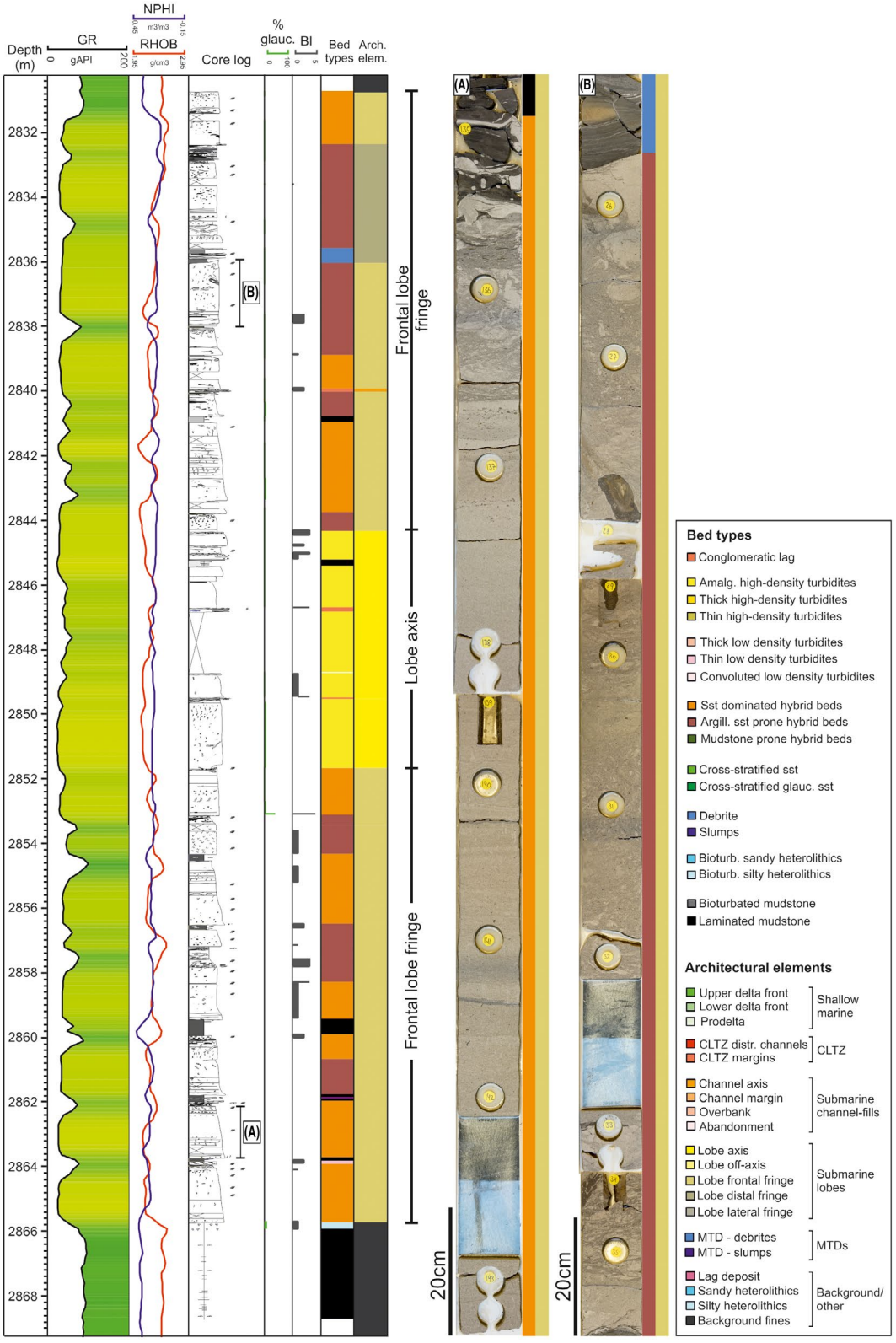

FIGURE 7 Lobe fringe type section of the Lysing Formation (well 6507/3-9S) with close-up core photographs of a sandstone-dominated hybrid bed in A) and an argillaceous sandstone-dominated hybrid bed in B). BI stands for bioturbation index and % glauc is the percentage of glauconite grains assessed visually

the Late-Mid Jurassic to Early Cretaceous, highlighted by the Base Cretaceous Unconformity (BCU) (Figure 2). Therefore, 55 Myr after active rifting ended, the syn-rift structural configuration still had an influence on sediment routing patterns despite the smoothing of topography during the early Cretaceous by the deposition of the Lyr and Lange Formations.

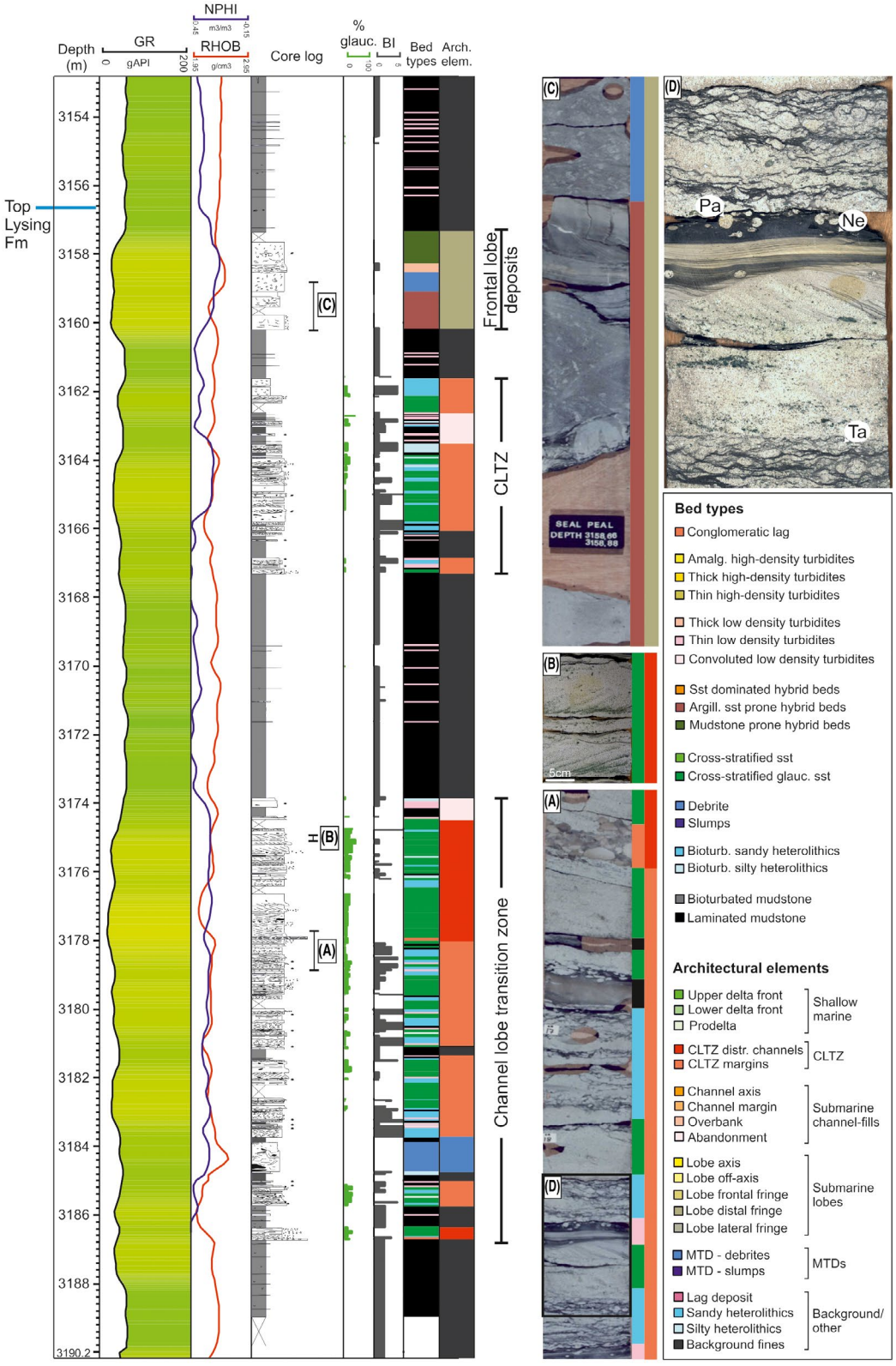

FIGURE 8 CLTZ type section of the Lysing Formation (well 6506/12-5) with close-up core photographs of bioturbated heterolithics, cross-stratified glauconitic sandstones and a hybrid bed shown in A), B) and C). D) Close-up of core section shown in A with dominant trace fossils highlighted. BI stands for bioturbation index and % glauc is the percentage of glauconite grains assessed visually

5 | BED TYPES

Based on the description of all available core data from the Lysing Formation, core facies that are commonly observed together were combined into 15 different bed types (Figure 4; Table 1). Structured and structureless sandstones and bipartite beds dominate the sandstone-prone bed types, and when combined make up 43.4% of the cored interval thickness, although there is a strong bias towards the sandier parts of the Lysing Formation as the mudstone-dominated parts have been rarely cored. The distribution of the architectural elements in all the cored and uncored wells described in Section 6 is more representative of the composition of the formation as a whole.

6 | ARCHITECTURAL ELEMENTS

The architectural elements in each cored and uncored well were interpreted based on the stratigraphic bed type distribution, bed type bounding surfaces, location of the well, and published seismic amplitude response (Fugelli & Olsen, 2007; Martinsen et al., 2005) (Figure 5). The architectural elements were calibrated between the core and wireline logs prior to interpretation of architectural elements in the uncored wells. Six groups of architectural elements were interpreted, which are described in more detail below.

6.1 | Submarine channel-fills

Submarine channels are conduits for sediment transport from the shelf to the basin-floor and occur on the slope, base-of-slope and proximal to medial parts of basin-floor fan systems (Carr & Gardner, 2000; Mutti & Normark, 1991; Walker, 1978). Channel-fills are interpreted in two wells in the study area, characterized by a >5-m thick, turbidite-dominated sandstone with blocky gamma ray signature in two uncored wells west of the Marulk High (6507/1-1) and south of the Heidrun High (6507/11-7) with evidence from seismic data confirming narrow conduits in those locations (Figure 5). They make up 2.1% of the Lysing Formation.

6.2 | Submarine lobes

Submarine lobes are subdivided into five different subenvironments: lobe axis, lobe off-axis, lobe frontal fringe, lobe lateral fringe and lobe distal fringe, based on bed types, sand content and degree of bed amalgamation (Kane et al., 2017; Prélat & Hodgson, 2013; Prélat et al., 2009). Submarine lobes make up 20.2% of the Lysing Formation (Figure 5), and are interpreted based on the abundance of amalgamated and thick-bedded structureless and structured sandstones (i.e. turbidites) and bipartite beds (i.e. hybrid beds), and lack of major erosion surfaces in the cores (bed types B1-2, D1-3). Published seismic amplitude maps clearly show the presence of multiple lobate features in the study area (Fugelli & Olsen, 2007; Martinsen et al., 2005), which is consistent with the presence of interpreted lobe deposits in core. Lobe axis deposits are distinguished by the presence of amalgamated and thick-bedded sandstones (i.e. high-density turbidites, bed types B1 and B2), whereas lobe off-axis deposits have more thin- to thick-bedded structured sandstones (i.e. low and high-density turbidites, bed types B2, C). Lobe fringe deposits are most abundant in the Lysing Formation, which is dominated by sandy to argillaceous bipartite beds (i.e. hybrid bed, bed types D1-2) and thin-bedded structures sandstones (i.e. low-density turbidites, bed type C) and have a serrated gamma ray signature (Figures 6 and 7). Lobe axis and lobe off-axis deposits are most abundant in the southern part of the Dønna Terrace, especially around wells 6506/6-1 and 6507/7-1 (Figure 5), which contain the thickest Lysing sandstone and have a less serrated gamma ray signature compared to the lobe fringes (Figure 6). Frontal and distal lobe deposits increase towards the south and reach past the Blåbjørn discovery (Figure 5).

6.3 | Channel-lobe transition zone

Channel-lobe transition zones (CLTZs) spatially separate well-defined channels up-dip from well-defined lobes down-dip, and form in relatively unconfined areas dominated by sediment bypass (Brooks et al., 2018; Mutti & Normark, 1987, 1991; Wynn et al., 2002). Changes in flow confinement, which commonly coincide with gradient changes, can cause flows to undergo hydraulic jumps due to variations in flow velocity and/or density (Pohl et al., 2019, 2020). This results in the presence of a distinctive assemblage of erosional features and depositional bedforms in the CLTZ (García & Parker, 1993; Hofstra et al., 2015; Ito, 2008; Komar, 1971; Macdonald et al., 2011; Mutti & Normark, 1987, 1991). Stratigraphic expressions of CLTZs are characterized by scour-fills, and thin and discontinuous structureless and structured sandstones dominated by ripple and climbing ripple lamination (García & Parker, 1993; Hofstra et al., 2015; Ito, 2008; Komar, 1971; Macdonald et al., 2011; Mutti & Normark, 1987, 1991). CLTZs can range in size from several 100s of metres to several kilometres in width and length and are very dynamic environments that expand, contract and migrate over time (Brooks et al., 2018).

The glauconite-rich cross-stratified bed types (G2) comprise 1.6% of the Lysing Formation (Figure 4). These deposits are mainly present around the Blåbjørn discovery in the cored

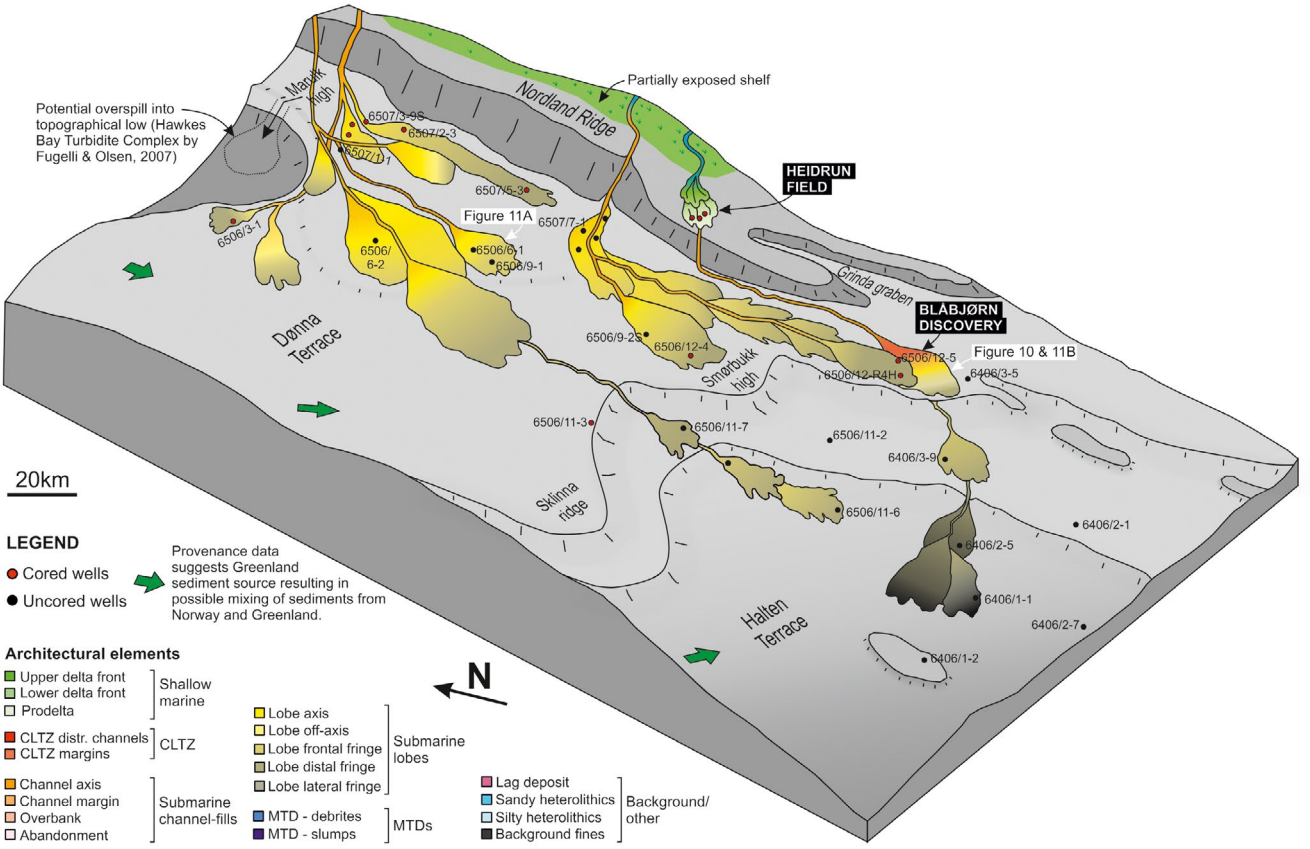

FIGURE 9 Palaeogeographic reconstruction of the Lysing Formation. The topography is based on the depth map in Figure 3A with the depositional bodies colour coded by their architectural element composition. Note that the fan-shaped bodies represent lobe complexes which are composed of several stacked lobes

wells 6506/12-5 and 6506/12-R4H (Figure 5) and were previously interpreted as tidally influenced deposits (Shanmugam et al., 1994) or traction reworked, confined and sediment bypass-dominated deposits in a deep-water setting (Lien et al., 2006). The presence of erosion surfaces and abundance of cross-stratified glauconite-rich sandstones interbedded with predominantly sandy bioturbated heterolithics (bed type H1) (Figure 8), as well as the absence of fine sand grain size and abundance of very fine and medium to coarse-grained sandstones, indicates that numerous sediment flows bypassed through this area (Stevenson et al., 2015). The co-deposition of quartz and glauconite sand grains in cross-stratified bedforms support the interpretation that the glauconite is reworked. The concentration of glauconite suggests that this area is relatively close to an updip shelfal source area of abundant in situ glauconite. A similar configuration is observed in the Palaeocene Siri canyon along the Danish-Norwegian North Sea boundary (Hamberg et al., 2005). Bioturbation intensity is high but the diversity is low suggesting that enough nutrients and organisms were transported to this area for bioturbation to occur but only limited number of trace-making organisms (*Palaeophycus, Nereites* and *Taenidium*) were able to thrive in such a high energy environment (Figure 8A). Therefore, the glauconite-rich cross-stratified bed types (G2) observed in the Lysing Formation are interpreted as bedforms that migrated, possibly at the base of scours, in a CLTZ setting.

6.4 | Mass transport deposits

Mass transport deposits (MTDs) are gravity-induced mass failures (Hampton et al., 1996; Kneller et al., 2016) and are rare (0.9%) in the Lysing Formation. Where present they comprise poorly sorted sandy mudstone (i.e. debrite, bed type E, Figure 8) and folded strata (i.e. slump, bed type F) deposits interpreted at the base of a channel-fill. Whilst not identified in the wells close to the Nordland Ridge, it is important to note that those areas could be prone to significant sediment collapse and remobilization, due to the steep topography. Hence, MTDs may be under-represented in this study.

6.5 | Background deposits/other heterolithics

Sandy and silty heterolithics (bed types H1-2) are very common in the Lysing Formation (13.1%), particularly in the

wells south of the Halten Terrace, and in wells 6506/11-3 and 6506/3-1 (Figure 5). The high bioturbation intensity suggests that enough nutrients and organisms were transported to this area to facilitate bioturbation. They can be associated with CLTZs but also occur in distal lobe fringe environments or may have been reworked by bottom currents (Brooks et al., 2018; Rebesco et al., 2014; Spychala, Hodgson, Prelat, et al., 2017).

Mudstones comprise 61.7% of the Lysing Formation and are composed of bioturbated and laminated mudstones (bed types I1-2). The Lysing Formation thickens and is increasingly mudstone-prone towards the south where the muds were deposited from a combination of hemiplegic suspension fallout and suspension fall-out from distal dilute turbidity currents introducing enough nutrients and oxygen to the environment to allow for bioturbation to take place.

6.6 | Shallow marine

Shallow marine deposits only comprise 0.4% of the Lysing Formation and are composed of amalgamated cross-bedded and ripple cross-laminated medium to very coarse-grained sandstones (bed type G1) interpreted as delta front deposits (van Cappelle et al., 2017). These deposits only occur in the cores of the Heidrun Field, which is interpreted as a partially exposed shelf during Lysing times (Fugelli & Olsen, 2007; Hastings, 1987).

7 | DISCUSSION

7.1 | Lysing Formation depositional model

The deposition of the Lysing Formation represented a major change in sediment supply to the Halten and Dønna terraces with the introduction of sand into the previously mud-dominated environment of the underlying upper Lange Formation. The abundance of lobe-related architectural elements intersected in the well datasets suggests that the Lysing Formation was dominated by submarine lobe deposits (Figure 9). Based on the cored and uncored wells through the Lysing Formation, at least three different deep-water systems were active on the Dønna and Halten terraces (Figure 9). Provenance data suggest that the sediments were largely sourced from Norway (Fonneland et al., 2004; Lien, 2005; Morton et al., 2005). However, in wells to the west of the study area, there is evidence of mixed sediment sources from Norway and Greenland, which were positioned 100–150 km from the study area in the Early and Late Cretaceous (Figure 1) (Fonneland et al., 2004; Lien, 2005; Morton et al., 2005). The sediment pathways are not possible to discern due to the lack of well and available 3D seismic reflection data, and more research is required to confirm the mixing of sediment sources (Figure 9).

The higher sandstone content due to the presence of some channel-fills, and the transition from proximal lobe axis and lobe off-axis deposits on the Dønna Terrace to distal frontal and lateral lobe fringe deposits towards the Halten Terrace (Figure 5), suggests the presence of a north-to-south oriented deep-water system (Figure 9). The sediment source for this system is likely to be the Nordland Ridge where several unconformities indicate that the ridge existed as an emergent high throughout the Cretaceous (Hastings, 1987). Combined with the thickness variations related to the subtle topography at the time of deposition observed on seismic reflection data (Figure 2) and the depth map (Figure 3A), the distribution of the architectural elements suggests that topographic lows to the west of, and above, the Marulk High (Figure 2B) acted as conduits for sediment transported southward. Published amplitude maps (Fugelli & Olsen, 2007; Martinsen et al., 2005), together with the distribution of architectural elements suggest that at least two-lobe complexes were present on the Dønna Terrace, which are up to 50 km in length (Figure 9). Subtle topography immediately to the west of the Nordland Ridge confines an elongate lobe complex that is interpreted to pinch out towards the south onto a high before reaching well 6507/7-1 (Figures 2D and 9), which was also identified by Fugelli and Olsen (2007). Cores suggest that this lobe complex is dominated by hybrid beds (Figure 5). This might be because the underlying Cretaceous interval was mud-prone, which enabled turbidity currents to entrain large quantities of mud. This primed the flows to readily transform into hybrid flows as they encountered narrow topographic confinement and rapidly decelerated. A similar character has been observed in the initiation of the submarine fan system in the Ross Formation, Ireland (Pierce et al., 2018) and in Braux, SE France, where flows have been shown to interact with confining slope topography (Patacci et al., 2014). The second lobe complex is less elongate and interpreted to compensationally stack in the area of wells 6506/6-1 and 6506/6-2 where there is an abundance of lobe axis and off-axis deposits (Figures 5 and 9) and a subtle thickening of the Lysing Formation can be seen on seismic reflection data associated with a subtle topographic low (Figure 2C). Fugelli and Olsen (2007) interpreted this system to be sourced from the south, but the regional southward dip of the slope (Figure 3A) makes a northern source more likely. Whether the two-lobe complexes are both sourced from the same input area of the Nordland Ridge remains unknown.

The sand content of the Lysing Formation increases towards the southern edge of the Dønna Terrace (Figure 5) with well 6507/7-1 containing the thickest Lysing sandstone (70-m thick; Figure 6). More accommodation may have been available due to subsidence along the nearby Heidrun-Smørbukk

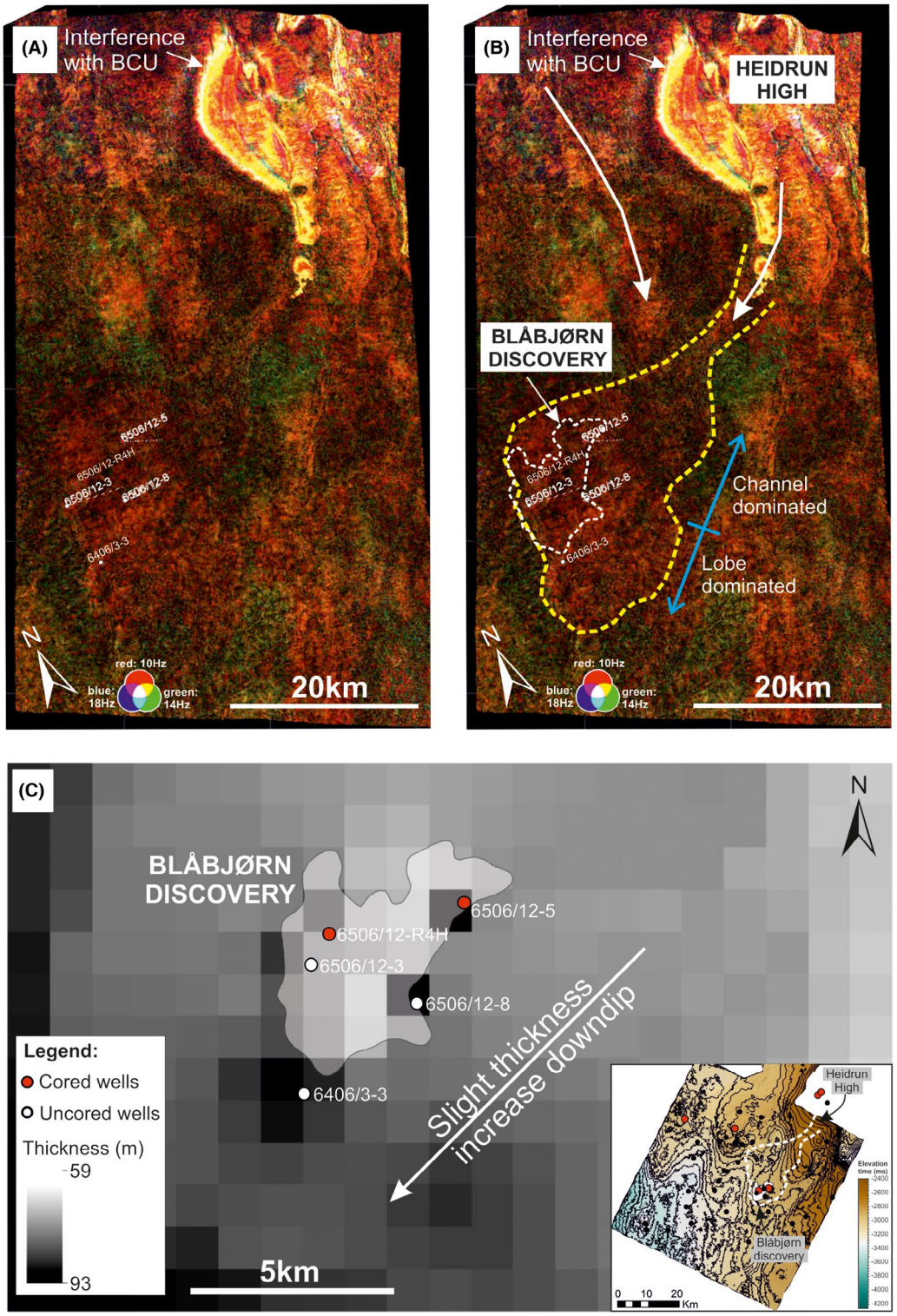

FIGURE 10 (A) Uninterpreted spectral decomposition image of the Heidrun and Blåbjørn area. (B) Interpreted spectral decomposition image of the Heidrun and Blåbjørn area. The lobate feature is highlighted in yellow and the outline of the Blåbjørn field is indicated. The white arrows show the interpreted sediment transport directions. (C) Zoomed in isochore map of the Lysing Formation around the Blåbjørn discovery indicating a slight thickening down-dip. The insert map shows where this area is located on the isochore map with the outline of the lobate feature also shown. The location is also indicated in Figure 9.

fault zone, or the location received sediments from the east through a canyon on the Nordland Ridge (Figure 9) (Fugelli & Olsen, 2007). The presence of lobe axis deposits in wells 6507/7-1 and 6507/7-15S (Figure 5) suggests that an eastern sediment source from the Nordland Ridge is likely. This system is interpreted to have prograded southwards given this

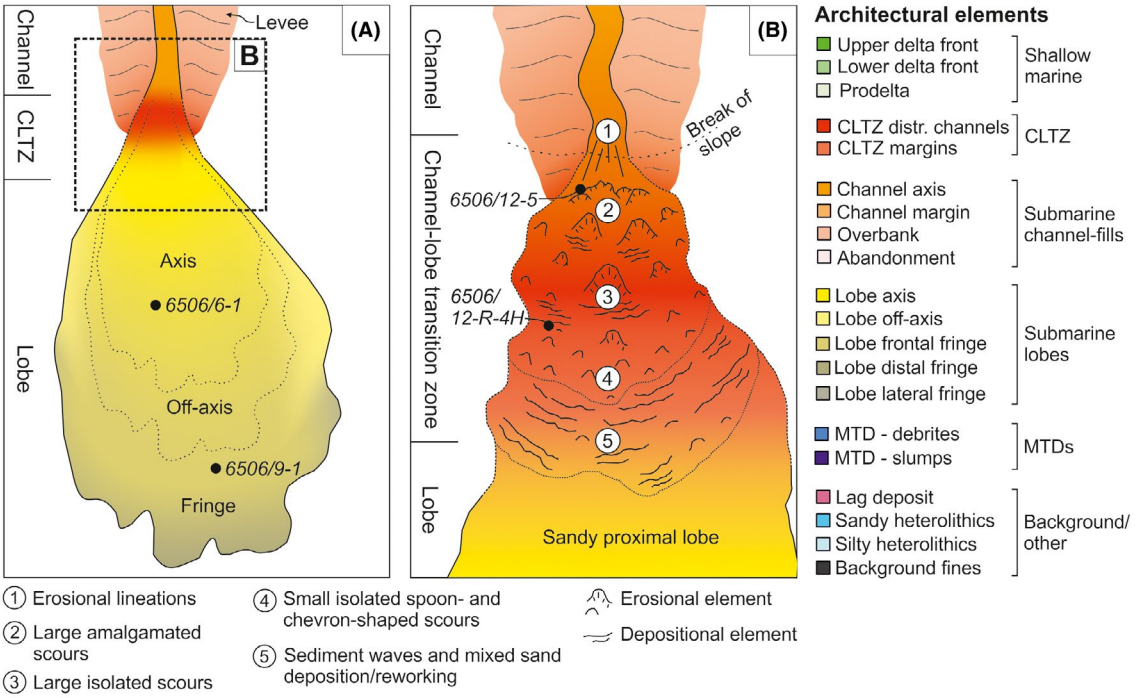

FIGURE 11 A) Cartoon illustrating the sub-environments within a single lobe (note that lobes stack to form lobe complexes). The location of this lobe is shown in Figure 9. B) Planform model of the CLTZ around the Blåbjørn discovery showing the spatial distribution of erosional and depositional elements. Erosional elements are closer to the channel-mouth and depositional elements appear in areas proximal to the lobe deposition (adapted from Hofstra, 2016; Wynn et al., 2002a). The location of the wells in the Blåbjørn discovery are indicated (illustrative only)

was the orientation of the slope and the increase in lobe fringe deposits in this direction (Figures 3A and 5). Lobe fringe deposits interpreted in well 6506/12-4 on the Smørbukk High are interpreted as the distal fringe of the lobe complex sourced from 6507/7-1 (Figure 9).

Towards the west, a topographic low is present between the Smørbukk High and Sklinna Ridge (Figure 3A) controlled by subsidence along the Smørbukk fault (Figure 2E). A north-to-south oriented seismic section shows that the southward dipping slope was stepped during deposition of the Lysing Formation (Figure 2A). The stepped slope resulted in sediments being deposited and compensationally stacked up-dip around wells 6506/6-2, 6506/6-1 and 6506/9-1 (Figures 2C and 9), before healing the topography and spilling into the next topographic low to the south (Figure 9). A broadly similar process has been interpreted from highly confined 'fill-and-spill' basins with ponded flows in the Gulf of Mexico (Prather et al., 1998) and from outcrops in the Cenozoic Alpine basin-fills (Pickering & Hilton, 1998; Sinclair, 2000; Sinclair & Tomasso, 2002). However, the configuration is more comparable to stepped slopes where the basal higher-concentration part of the flow is deposited on the step to form intraslope lobes, and the upper lower-concentration part of the flow is stripped and travels further downstream (e.g. Spychala et al., 2015). The wells positioned in the topographic low have two distinct sandstone-prone packages (e.g. wells 6506/11-7 and 6506/11-4 ST2, Figure 6) and are interpreted as frontal lobe hybrid beds that represent the distal extent of the main north-to-south oriented deep-water system. The two packages may either represent multiple sediment pulses that reached this area from the north, or indicate the interaction between the north-to-south trending deep-water system and an east-to-west trending system sourced from the Heidrun High (Figure 9). The cored well 6506/11-3 is positioned on the topographic high to the west (Figure 9), and is dominated by bioturbated sandy and silty heterolithics (Figure 6). These are interpreted to be the very distal lateral fringe deposits of the north-to-south trending lobe complex occupying the adjacent topographic low.

From the Dønna to the Halten Terrace, the slope steps down southward, which corresponds to the thickest part of the Lysing Formation (Figure 3B). The increase in thickness is also associated with an increase in mudstone and heterolithics interpreted to represent distal lobe-related deposits (e.g. well 6406/2-1 in Figures 6 and 9).

7.2 | Blåbjørn discovery depositional model

To the east and south-east of the Smørbukk high, the wells in the Heidrun field and the Blåbjørn discovery comprise a variety of architectural elements (Figure 5). The Lysing

Formation has not been previously interpreted in the Heidrun field (Moscardelli et al., 2013). However, a new biostratigraphic interpretation supports the presence of an ~8-m-thick sandstone-prone Lysing Formation in the Heidrun field above Jurassic sandstones separated by an unconformity (Figure 6, well 6507/7-A-35). The cores of the Lysing Formation in the Heidrun field suggest a shallow marine depositional environment, with the Nordland Ridge interpreted as an emergent high due to uplift as a result of Late Cretaceous tectonism (Fugelli & Olsen, 2007; Hastings, 1987). Figure 2F shows a stepped slope from the Heidrun field to the Blåbjørn discovery and further southwest, with a spectral decomposition image (Figure 10A,B) indicating a northeast-southwest oriented lobe-shaped feature that extends towards the Blåbjørn discovery. This configuration supports an additional sediment input point, and that the Heidrun deposits are the shallow water expression of the likely sediment source area for the Blåbjørn discovery (Figure 9). The abundance of resedimented glauconite in the Blåbjørn wells supports a shallow marine sediment source as glauconite forms exclusively in the uppermost section of the marine sedimentary column, where rates of sediment accumulation are low (Amorosi, 2012; McCracken et al., 1996).

The Lysing Formation in the Blåbjørn discovery in the cored wells 6506/12-5 and 6506/12-R4H is composed of cross-stratified glauconitic sandstones interbedded with bioturbated heterolithics (Figure 8), which have been discussed and interpreted previously as either tidally influenced deposits (Shanmugam et al., 1994) or traction reworked, confined and sediment bypass-dominated deposits in a deep-water setting (Lien et al., 2006). The latter supports our interpretation that these sediments were deposited in scour- or distributary channel-fills in a CLTZ above a stepped slope profile, which has distinctly different architectural elements to lobe complexes (Figure 11). The stepped slope resulted in the accumulation of sediment in the Blåbjørn discovery before spilling south-westward into the next topographic low forming lobes that may have reached as far as well 6406/2-5 (Figure 9).

The base of the core in well 6506/12-5, which coincides with the base of the sandstone interval, show the presence of a thin conglomerate lag deposit and a debrite below a 10-m-thick interval of cross-stratified glauconitic sandstones interbedded with bioturbated heterolithics (Figures 6 and 8). This is interpreted as the base of a distributary channel-fill in a proximal part of a CLTZ (Figure 11B). The cross-stratified sandstones interbedded with bioturbated heterolithics indicate that multiple sediment bypass-dominated flows reworked and deposited sediment in this area, which is typical for scour-fills in CLTZs (Brooks et al., 2018; Hofstra et al., 2015) (Figure 11B). The gamma ray signature of the surrounding uncored wells in the north-eastern section of the Blåbjørn discovery show a similarly abrupt start to the sandstone-prone interval. Towards the south-western part of the Blåbjørn discovery, and in the cored well 6506/12-R4H, the gamma ray signature at the base of the sandstone package changes, showing three sandstone beds with a fining-upwards signature in each bed similar to the gamma ray signature seen in hybrid beds in other wells in the study area (Figure 6). These beds are not cored in well 6506/12-R4H, but the change in the gamma ray signature may indicate an increase in lobe-related hybrid beds, placing this well in the area of a CLTZ where lobe deposits are commonly incised and reworked (Figure 11B). The scour-fills present above these lobe deposits may indicate that the system was progradational. The change from distributary channel-fill deposits to more lobe-related deposits is accompanied by an increase in thickness of the Lysing Formation down-dip (Figure 10C), which is an expected change from more sediment bypass-dominated proximal CLTZ to a more deposition-dominated distal part of a CLTZ (Figure 11B). Based on the wells the CLTZ is constrained to a 5 × 3 km area, comparable to that reported in Brooks et al. (2018).

The core in well 6506/12-5, as well as the gamma ray signature in the Blåbjørn wells, shows the presence of one or more 1- to 3-m-thick hybrid beds at the top of the Lysing Formation separated from the underlying glauconitic cross-stratified sandstones by a 1- to 4-m-thick mudstone (Figures 6 and 8). If these hybrid beds are related to the underlying deposits, mud would have had to be incorporated at a very early stage of the flows evolution and the hybrid beds deposited in a relatively proximal position. Mud-prone hybrid beds usually develop over longer distances and are deposited on lobe fringes (e.g. Kane et al., 2017; Spychala et al., 2017), making it unlikely that they are related to the underlying deposits. Instead, they are interpreted to represent the frontal lobe deposits of the system sourced from the Nordland Ridge at well 6507/7-1 (Figure 9), with the spectral decomposition data supporting an additional northern sediment source in this area (Figure 10A,B).

7.3 | Interaction of transverse and axial deep-water systems

Axial (longitudinal) or transverse sediment supply to the syn-rift structural grain impacts the architecture of post-rift successions. In the Lysing Formation, the transgression of the lateral basin margin and the infill of accommodation resulted in a transition from dominantly axial to transverse sediment routing. This led to the interaction of submarine lobe complexes from different source areas. The transition from axial to transverse sediment supply can result in the stratigraphic juxtaposition of architectural elements (i.e. lobe axis, distal lobe fringe and CLTZ deposits) that represent different parts of a deep-water system. This results in a composite and complicated stratigraphic architecture across a small area.

Existing marine rift-basin models emphasize syn-rift stages dominated by axial sediment transport when sediment routing is linked to normal fault growth (McArthur et al., 2016), whereas transverse sediment transport dominates during the post-rift or passive margin stages. However, the temporal and spatial interactions of axial and transverse sediment supply are poorly understood. In the Gulf of Corinth, Greece, studies of exhumed systems have shown that during syn-rift stages a transverse system dominated by mass flows can impact the sediment routing of the contemporaneous axial system (Cullen et al., 2020). In the post-rift Central North Sea, provenance studies have shown that axial systems can interfinger with transverse systems (Kilhams et al., 2014). In this study, the juxtaposition of lobe fringe and CLTZ deposits in the area around the Blåbjørn discovery illustrates the presence of contemporaneous axial and transverse sediment transport systems that formed intricate stratigraphic architectures (Figure 9). These coeval systems formed as a result of multiple sediment input points and the gradual infilling of subtle topography that guided sediment routing patterns, has had a major impact on the depositional architecture of the system.

In other types of basins, such as foreland basins, a temporal change from dominantly axial (or longitudinal) to dominantly transverse sediment routing, represents early underfilled (Flysch) and late overfilled (Molasse) phases as sedimentation outpaces flexural subsidence (Covey, 1986). Some studies of deep-marine successions in foreland basinfills have identified contemporaneous axial and transverse supply. For example in the Oligocene-early Miocene Molasse Basin, Austria, detrital zircon geochronology has been used to constrain the relative sediment contributions of transverse tributaries (Sharman et al., 2018). However, the evolution of foreland basins from underfilled to overfilled is characterized by an evolution from deep-marine to non-marine sedimentation. In contrast, in many post-rift settings thermal subsidence maintains a deep-marine setting, and the interplay of axial to transverse is related to the progressive healing of inherited topography.

In post-rift settings, the sediment transport distances vary between axial and transverse systems depending on the topography they encounter. In the case of the Lysing Formation, the axial system transported sediments over an estimated 100 km southward whilst the sediment transport distance of the transverse systems was 30–50 km. The interaction between axial and transverse systems may improve reservoir connectivity between lobe complexes, but the stacking of architectural elements from different systems will make predictions of reservoir quality challenging. Awareness of the complexity created by coeval axial and transverse systems in both syn- and post-rift settings is crucial when trying to predict reservoir quality and distribution in these settings.

8 | CONCLUSIONS

This study utilizes an extensive cored and uncored well dataset with seismic reflection data to describe the distribution of architectural elements in the Cretaceous Lysing Formation, offshore Norway. The relatively thin sandstone interval in the Lysing Formation limits the seismic data resolution making a detailed study of the architectural element distribution in the wells crucial to better define the depositional environment and reservoir distribution. A regional trend from more proximal architectural elements in the north to more distal architectural elements in the south indicates the presence of a large north-to-south oriented axial submarine fan system. However, the juxtaposition of different architectural elements (e.g. CLTZ and lobe fringe deposits) representing different parts of several deep-water systems highlights the presence of coeval locally sourced transverse sediment sources. Subtle post-rift topography influenced sediment pathways and architectural element distribution. However, this study is a unique example of a regional-scale post-rift deep-water model with synchronous active systems sourced from multiple entry points and following subtle topography inherited from syn-rift topography (that ended 55 Myr earlier), which can contribute to the refinement of prevailing tectono-stratigraphic models.

ACKNOWLEDGEMENTS

The authors thank Equinor for sponsoring and allowing to publish this work as well as helping with the interpretation and seismic mapping. We also thank the Åsgard team and partners as well as PGS for allowing us to publish. Martin Bartenbach and Maarten Papo had essential input in the Blåbjørn interpretation and we also thank them for their logistical support. LH wrote the manuscript with edits and contributions made by all co-authors. All co-authors were involved in the core logging with the seismic interpretation done by CT. Euan Soutter and an anonymous reviewer are thanked for their constructive reviews which emphasized the broader significance of the study. The authors have no conflict of interest to declare.

PEER REVIEW

The peer review history for this article is available at https://publons.com/publon/10.1111/bre.12555.

DATA AVAILABILITY STATEMENT

The data that support the findings of this study cannot be shared due to privacy restrictions.

ORCID

L. A. S. Hansen https://orcid.org/0000-0002-5013-132X
D. M. Hodgson https://orcid.org/0000-0003-3711-635X

REFERENCES

Amorosi, A. (2012). The occurrence of glaucony in the stratigraphic record: Distribution patterns and sequence-stratigraphic significance. In *Int. Assoc. Sedimentol. Spec. Publ.* (Vol. *45*, pp. 37–54).

Blystad, P., Brekke, H., Faerseth, R. B., Larsen, B. T., Skogseid, J., & Torudbakken, B. (1995). Structural elements of the Norwegian continental shelf: Part II. The Norwegian Sea Region. *Norw. Petr. Dir.-Bull*. 8.

Brekke, H., Dahlgren, S., Nyland, B., & Magnus, C. (1999). The prospectivity of the Vøring and Møre basins on the Norwegian Sea conti- nental margin. In A. J. Fleet & S. A. Boldy (Eds.), *Petroleum geology of Northwest Europe: Proceedings of the 5th conference* (pp. 41–61).

Brekke, H., Sjulstad, H. I., Magnus, C., & Williams, R. W. (2001). Sedimentary environments offshore Norway - An overview. In O. J. Martinsen & T. Dreyer (Eds.), *Sedimentary environments offshore Norway - Palaeozoic to recent*. NPF Special Publication (pp. 7–37).

Brooks, H. L., Hodgson, D., Brunt, R. L., Peakall, J., Hofstra, M., & Flint, S. (2018). Deep-water channel-lobe transition zone dynamics: Processes and depositional architecture, an example from the Karoo Basin, South Africa. *GSA Bulletin*, *130*(9–10), 1723–1746.

Carr, M., & Gardner, M. (2000). Portrait of a basin-floor fan for sandy deepwater systems, Permian lower Brushy Canyon Formation, west Texas. In A. Bouma & C. Stone (Eds.), *Fine-grained turbidite systems: American Association of Petroleum Geologists*. Memoir 72, SEPM Special Publications 68 (pp. 215–232).

Covey, M. (1986). The evolution of foreland basins to steady state: Evidence from the western Taiwan foreland basin. *International Association of Sedimentologists Special Publication*, *8*, 77–90.

Cullen, T., Collier, R. E., Gawthorpe, R. L., Hodgson, D. M., & Barrett, B. J. (2020). Axial and transverse deep-water sediment supply to syn-rift fault terraces: Insights from the West Xylokastro Fault Block, Gulf of Corinth, Greece. *Basin Research*, *32*, 1105–1139. https://doi.org/10.1111/bre.12416

Dodd, T. J. H., McCarthy, D. J., & Richards, P. C. (2019). A depositional model for deep-lacustrine, partially confined, turbidite fans: Early Cretaceous, North Falkland Basin. *Sedimentology*, *66*, 53–80. https://doi.org/10.1111/sed.12483

Doré, A. G., & Lundin, E. R. (1996). Cenozoic compressional structures on the NE Atlantic margin: Nature, origin and potential significance for hydrocarbon exploration. *Petroleum Geoscience*, *2*, 299–311. https://doi.org/10.1144/petgeo.2.4.299

Elliott, G. M., Wilson, P., Jackson, C., Gawthorpe, R., Michelsen, L., & Sharp, I. R. (2012). The linkage between fault throw and footwall scarp erosion patterns: An example from the Bremstein Fault Complex, offshore Mid-Norway. *Basin Research*, *24*(2), 180–197. https://doi.org/10.1111/j.1365-2117.2011.00524.x

Færseth, R. B., & Lien, T. (2002). Cretaceous evolution in the Norwegian Sea - A period characterized by tectonic quiescence. *Marine and Petroleum Geology*, *19*(8), 1005–1027. https://doi.org/10.1016/S0264-8172(02)00112-5

Fjellanger, E., Surlyk, F., Wamsteeker, L. C., & Midtun, T. (2005). Upper cretaceous basin-floor fans in the Vøring Basin, Mid Norway shelf. In B. T. Wandås, J. P. Nystuen, E. Eide, & F. Gradstein (Eds.), *Proceedings of the Norwegian Petroleum Society Conference* (pp. 135–164). Norwegian Petroleum Society Special Publications.

Fonneland, H. C., Lien, T., Martinsen, O. J., Pedersen, R. B., & Košler, J. (2004). Detrital zircon ages: A key to understanding the deposition of deep marine sandstones in the Norwegian Sea. *Sedimentary Geology*, *164*(1–2), 147–159. https://doi.org/10.1016/j.sedgeo.2003.09.005

Fugelli, E., & Olsen, T. (2007). Delineating confined slope turbidite systems offshore mid-Norway: The Cretaceous deep-marine Lysing Formation. *AAPG Bulletin*, *91*(11), 1577–1601. https://doi.org/10.1306/07090706137

García, M., & Parker, G. (1993). Experiments on the entrainment of sediment into suspension by a dense bottom current. *Journal of Geophysical Research*, *98*(3), 4793–4807. https://doi.org/10.1029/92JC02404

Gawthorpe, R. L., & Hurst, J. M. (1993). Transfer zones in extensional basins: Their structural style and influence on drainage development and stratigraphy. *Journal of the Geological Society (London)*, *150*, 1137–1152. https://doi.org/10.1144/gsjgs.150.6.1137

Gibbs, A. D. (1984). Structural evolution of extensional basin margins. *Journal of the Geological Society (London)*, *141*, 609–620. https://doi.org/10.1144/gsjgs.141.4.0609

Hadlari, T., Midwinter, D., Galloway, J. M., Dewing, K., & Durbano, A. M. (2016). Mesozoic rift to post-rift tectonostratigraphy of the Sverdrup Basin, Canadian Arctic. *Marine and Petroleum Geology*, *76*, 148–158. https://doi.org/10.1016/j.marpetgeo.2016.05.008

Hamberg, L., Dam, G., Wilhelmson, C., & Ottesen, T. G. (2005). Paleocene deep-marine sandstone plays in the Siri Canyon, offshore Denmark–southern Norway. *Geological Society, London, Petroleum Geology Conference Series*, *6*, 1185–1198. https://doi.org/10.1144/0061185

Hampton, M. A., Lee, H., & Locat, J. (1996). Submarine landslides. *Reviews of Geophysics*, *34*, 33–59. https://doi.org/10.1007/978-3-319-57852-1_13

Hastings, D. S. (1987). Sand-prone facies in the Cretaceous of Mid-Norway. In J. Brooks & K. W. Glennie (Eds.), *Petroleum geology of Northwest Europe* (pp. 1065–1078). Graham and Trotman.

Haughton, P. D. W., Barker, S. P., & McCaffrey, W. D. (2003). 'Linked" debrites in sand-rich turbidite systems – Origin and significance. *Sedimentology*, *50*, 459–482. https://doi.org/10.1046/j.1365-3091.2003.00560.x

Hofstra, M. (2016). *The stratigraphic record of submarine channel-lobe transition zones*. University of Leeds. Unpublished PhD thesis.

Hofstra, M., Hodgson, D., Peakall, J., & Flint, S. (2015). Giant scour-fills in ancient channel-lobe transition zones: Formative processes and depositional architecture. *Sedimentary Geology*, *329*, 98–114. https://doi.org/10.1016/j.sedgeo.2015.09.004

Ito, M. (2008). Downfan transformation from turbidity currents to debris flows at a channel-to-lobe transitional zone: The lower Pleistocene Otadai Formation, Boso Peninsula, Japan. *Journal of Sedimentary Research*, *78*(10), 668–682. https://doi.org/10.2110/jsr.2008.076

Jackson, C., Barber, G. P., & Martinsen, O. J. (2008). Submarine slope morphology as a control on the development of sand-rich turbidite depositional systems: 3D seismic analysis of the Kyrre Fm (Upper Cretaceous), Maloy Slope, offshore Norway. *Marine and Petroleum Geology*, *25*(8), 663–680. https://doi.org/10.1016/j.marpetgeo.2007.12.007

Kane, I., Pontén, A. S. M., Vangdal, B., Eggenhuisen, J., Hodgson, D., & Spychala, Y. T. (2017). The stratigraphic record and processes of turbidity current transformation across deep-marine lobes. *Sedimentology*, *64*, 1236–1273. https://doi.org/10.1111/sed.12346

Kilhams, B., Morton, A., Borella, R., Wilkins, A., & Hurst, A. (2014). Understanding the provenance and reservoir quality of the Sele

Formation sandstones of the UK Central Graben utilizing detrital garnet suites. *Geological Society, London, Special Publications*, *386*, 129–142. https://doi.org/10.1144/SP386.16

Kneller, B., Dykstra, M., Fairweather, L., & Milana, J. P. (2016). Mass-transport and slope accommodation: Implications for turbidite sandstone reservoirs. *AAPG Bulletin*, *100*(2), 213–235. https://doi.org/10.1306/09011514210

Komar, P. (1971). Hydraulic jumps in turbidity currents. *Geological Society of America Bulletin*, *82*, 1477–1488. https://doi.org/10.1130/0016-7606(1971)82

Leinfelder, R. R., Wilson, R., & Chris, L. (1998). Third-order sequences in an upper Jurassic rift-related second-order sequence, Central Lusitanian Basin, Portugal. In P. C. Graciansky, J. Hardenbol, T. Jacquin, & P. R. Vail (Eds.), *Mesozoic and Cenozoic sequence stratigraphy of European basins* (pp. 507–525). SEPM.

Lien, T. (2005). From rifting to drifting: Effects on the development of deep-water hydrocarbon reservoirs in a passive margin setting, Norwegian Sea. *Norwegian Journal of Geology*, *85*(4), 319–332.

Lien, T., Midtbø, R. E., & Martinsen, O. J. (2006). Depositional facies and reservoir quality of deep-marine sandstones in the Norwegian Sea. *Norwegian Journal of Geology*, *86*(2), 71–92.

Macdonald, H. A., Peakall, J., Wignall, P. B., & Best, J. (2011). Sedimentation in deep-sea lobe-elements: Implications for the origin of thickening-upward sequences. *Journal of the Geological Society, London*, *168*, 319–331. https://doi.org/10.1144/0016-76492010-036

Martinsen, O. J., Lien, T., & Jackson, C. (2005). Cretaceous and Palaeogene turbidite systems in the North Sea and Norwegian Sea Basins: source, staging area and basin physiography controls on reservoir development. In A. G. Doré & B. A. Viking (Eds.), Petroleum geology: North-West Europe and global perspectives – Proceedings of the 6th petroleum geology conferences (pp. 1147–1164). London: Geological Society.

McArthur, A., Hartley, A. J., Archer, S. G., Jolley, D. W., & Lawrence, H. M. (2016). Spatiotemporal relationships of deep-marine, axial, and transverse depositional systems from the synrift Upper Jurassic of the central. *North Sea*, *9*(9), 1469–1500. https://doi.org/10.1306/04041615125

McCracken, S. R., Compton, J., & Hicks, K. (1996). Sequence-stratigraphic significance of glaucony-rich lithofacies at site 903. In *Proceedings of the Ocean Drilling Program* (Vol. *150*(1981)). http://www-odp.tamu.edu/publications/150_SR/VOLUME/CHAPTERS/sr150_10.pdf

Morley, C. K., Nelson, R. A., Patton, T. L., & Munn, S. G. (1990). Transfer zones in the East African rift system and their relevance to hydrocarbon exploration in rifts. *AAPG Bulletin*, *74*, 1234–1253.

Morton, A. C., Whitham, A. G., & Fanning, C. M. (2005). Provenance of Late Cretaceous to Paleocene submarine fan sandstones in the Norwegian Sea: Integration of heavy mineral, mineral chemical and zircon age data. *Sedimentary Geology*, *182*(1–4), 3–28. https://doi.org/10.1016/j.sedgeo.2005.08.007

Mosar, J., Eide, E. A., Osmundsen, P. T., Sommaruga, A., & Torsvik, T. H. (2002). Greenland - Norway separation: A geodynamic model for the North Atlantic. *Norwegian Journal of Geology*, *82*, 281–298.

Moscardelli, L., Ramnarine, S. K., Wood, L., & Dunlap, D. B. (2013). Seismic geomorphological analysis and hydrocarbon potential of the Lower Cretaceous Cromer Knoll Group, Heidrun field, Norway. *AAPG Bulletin*, *97*(8), 1227–1248. https://doi.org/10.1306/02081312155

Muravchik, M., Henstra, G. A., Eliassen, G. T., Gawthorpe, R. L., Leeder, M., Kranis, H., Skourtsos, E., & Andrews, J. (2020). Deep-water sediment transport patterns and basin floor topography in early rift basins: Plio-Pleistocene syn-rift of the Corinth Rift, Greece. *Basin Research*, *32*(5), 1194–1222. https://doi.org/10.1111/bre.12423

Mutti, E., & Normark, W. (1987). Comparing examples of modern and ancient turbidite systems: Problems and concepts. In J. Leggett, & G. Zuffa (Eds.), *Marine clastic sedimentology* (pp. 1–38). Graham and Trotman.

Mutti, E., & Normark, W. (1991). An integrated approach to the study of turbidite systems. In P. Weimer, & M. Link (Eds.), *Seismic facies and sedimentary processes of submarine fans and turbidite systems* (pp. 75–106). Springer-Verlag.

Patacci, M., Haughton, P., & McCaffrey, W. D. (2014). Rheological complexity in sediment gravity flows forced to decelerate against a confining slope, Braux, SE France. *Journal of Sedimentary Research*, *84*(4), 270–277. https://doi.org/10.2110/jsr.2014.26

Pickering, K. T., Clark, J. D., Smith, R. D. A., Hiscott, R. N., Ricci Lucchi, F., & Kenyon, N. H. (1995). Architectural element analysis of turbidite systems, and selected topical problems for sand-prone deep-water systems. *Atlas of Deep Water Environments*, *1–10*, https://doi.org/10.1007/978-94-011-1234-5_1

Pickering, K. T., & Hilton, V. C. (1998). *Turbidite systems of southeast France: Application to hydrocarbon prospectivity*. Vallis Press.

Pierce, C. S., Haughton, P. D. W., Shannon, P. M., Pulham, A. J., Barker, S. P., & Martinsen, O. J. (2018). Variable character and diverse origin of hybrid event beds in a sandy submarine fan system, Pennsylvanian Ross Sandstone Formation, Western Ireland, *Sedimentology*, *65*, 952–992, https://doi.org/10.1111/sed.12412

Pohl, F., Eggenhuisen, J. T., Cartigny, M. J. B., Tilston, M. C., de Leeuw, J., & Hermidas, N. (2020). The influence of a slope break on turbidite deposits: An experimental investigation. *Marine Geology*, *424*(February), https://doi.org/10.1016/j.margeo.2020.106160

Pohl, F., Eggenhuisen, J. T., Tilston, M., & Cartigny, M. J. B. (2019). New flow relaxation mechanism explains scour fields at the end of submarine channels. *Nature Communications*, *10*(1), 1–8. https://doi.org/10.1038/s41467-019-12389-x

Prather, B. E., Booth, J. R., Steffens, G. S., & Craig, P. A. (1998). Classification, lithologic calibration, and stratigraphic succession of seismic facies of intraslope basins, deep-water Gulf of Mexico. *AAPG Bulletin*, *82*(5 A), 701–728. https://doi.org/10.1306/1d9bc5d9-172d-11d7-8645000102c1865d

Prélat, A., & Hodgson, D. (2013). The full range of turbidite bed thickness patterns in submarine lobes: Controls and implications. *Journal of the Geological Society*, *170*(1), 209–214. https://doi.org/10.1144/jgs2012-056

Prélat, A., Hodgson, D., & Flint, S. (2009). Evolution, architecture and hierarchy of distributary deep-water deposits: A high-resolution outcrop investigation from the Permian Karoo Basin, South Africa. *Sedimentology*, *56*(7), 2132–2154. https://doi.org/10.1111/j.1365-3091.2009.01073.x

Prosser, S. (1993). Rift-related linked depositional systems and their seismic expression. In G.D. Williams & A. Dobb (Eds.), *Tectonics and seismic sequence stratigraphy* (pp. 35–66). London: Geological Society London, Special Publications.

Rebesco, M., Hernández-Molina, F. J., Van Rooij, D., & Wåhlin, A. (2014). Contourites and associated sediments controlled by deep-water circulation processes: State-of-the-art and future considerations. *Marine Geology*, *352*, 111–154. https://doi.org/10.1016/j.margeo.2014.03.011

Shanmugam, G., Lehtonen, L. R., Straume, T., Syvertsen, S. E., & Hodgkinson, R. J. (1994). Slump and debris-flow dominated upper slope facies in the Cretaceous of the Norwegian and Northern North Seas (61–67° N): Implications for sand distribution 1. *AAPG Bulletin*, *78*(6), 910–937.

Sharman, G. R., Hubbard, S. M., Covault, J. A., Hinsch, R., Linzer, H. G., & Graham, S. A. (2018). Sediment routing evolution in the North Alpine Foreland Basin, Austria: Interplay of transverse and longitudinal sediment dispersal. *Basin Research*, *30*(3), 426–447. https://doi.org/10.1111/bre.12259

Sinclair, H. D. (2000). Delta-fed turbidites infilling topographically complex basins: A new depositional model for the Annot Sandstones, SE France. *Journal of Sedimentary Research*, *70*, 504–519. https://doi.org/10.1306/2DC40923-0E47-11D7-8643000102C1865D

Sinclair, H. D., & Tomasso, M. (2002). Depositional evolution of confined turbidite basins. *Journal of Sedimentary Research*, *72*(4), 451–456. https://doi.org/10.1306/111501720451

Skogseid, J., Planke, S., Faleide, J. I., Pedersen, T., Eldholm, O., & Neverdal, F. (2000). NE Atlantic continental rifting and volcanic margin formation. *Dynamics of the Norwegian Margin. Geological Society, London, Special Publication*, *167*, 295–326. https://doi.org/10.1144/GSL.SP.2000.167.01.12

Southern, S. J., Kane, I., Warchoł, M. J., Porten, K., & McCaffrey, W. D. (2017). Hybrid event beds dominated by transitional-flow facies: Character, distribution and significance in the maastrichtian springar formation, north-west vøring basin, Norwegian Sea. *Sedimentology*, *64*(3), 747–776. https://doi.org/10.1111/sed.12323

Spychala, Y. T., Hodgson, D., Flint, S., & Mountney, N. P. (2015). Constraining the sedimentology and stratigraphy of submarine intraslope lobe deposits using exhumed examples from the Karoo Basin, South Africa. *Sedimentary Geology*, *322*, 67–81. https://doi.org/10.1016/j.sedgeo.2015.03.013

Spychala, Y. T., Hodgson, D., & Lee, D. R. (2017). Autogenic controls on hybrid bed distribution in submarine lobe complexes. *Marine and Petroleum Geology*, *88*, 1078–1093. https://doi.org/10.1016/j.marpetgeo.2017.09.005

Spychala, Y. T., Hodgson, D., Prelat, A., Kane, I., Flint, S., & Mountney, N. (2017). Frontal and lateral submarine lobe fringes: Comparing sedimentary facies, architecture and flow processes. *Journal of Sedimentary Research*, *87*(January), 75–96. https://doi.org/10.2110/jsr.2017.2

Stevenson, C., Jackson, C., Hodgson, D., Hubbard, S., & Eggenhuisen, J. (2015). Deep-water sediment bypass. *Journal of Sedimentary Research*, *85*, 1058–1081. https://doi.org/10.2110/jsr.2015.63

Swiecicki, T., Gibbs, P. B., Farrow, G. E., & Coward, M. P. (1998). A tectonostratigraphic framework for the Mid-Norway region. *Marine and Petroleum Geology*, *15*, 245–276. https://doi.org/10.1016/S0264-8172(97)00029-9

Torsvik, T. H., & Cocks, L. R. M. (2005). Norway in space and time: A centennial cavalcade. *Norwegian Journal of Geology*, *85*, 73–86.

van Cappelle, M., Ravnas, R., Hampson, G. J., & Johnson, H. D. (2017). Depositional evolution of a progradational to aggradational, mixed-influenced deltaic succession: Jurassic Tofte and Ile formations, southern Halten Terrace, offshore Norway. *Marine and Petroleum Geology*, *80*, 1–22. https://doi.org/10.1016/j.marpetgeo.2016.11.013

Walker, R. (1978). Deep-water sandstone facies and ancient submarine fans: Models for exploration for stratigraphic traps. *AAPG Bulletin*, *62*(6), 932–966. https://doi.org/10.1306/C1EA4F77-16C9-11D7-8645000102C1865D

Wynn, R., Kenyon, N. H., Masson, D., Stow, D., & Weaver, P. (2002). Characterization and recognition of deep-water channel-lobe transition zones. *AAPG Bulletin*, *86*, 1441–1462.

Wynn, R., Piper, D., & Gee, M. (2002). Generation and migration of coarse-grained sediment waves in turbidity current channels and channel–lobe transition zones. *Marine Geology*, *192*(1–3), 59–78. https://doi.org/10.1016/S0025-3227(02)00549-2

How to cite this article: Hansen LAS, Hodgson DM, Pontén A, Thrana C, Obradors Latre A. Mixed axial and transverse deep-water systems: The Cretaceous post-rift Lysing Formation, offshore Norway. *Basin Res*. 2021;00:1–23. https://doi.org/10.1111/bre.12555